

1992

**THE ONSET OF THE PINDOS FORELAND BASIN
IN EPIRUS (N.W. GREECE).**

**F.J.C. Peeters
R.P. Hoek**

Laboratory of
Palaeobotany and Palynology
Heidelberglaan 2
3584 CS Utrecht

THE ONSET OF THE PINDOS FORELAND BASIN IN EPIRUS (NORTHWEST GREECE)

ABSTRACT

An integrated study of dinoflagellate cyst distributions, palaeocurrent analysis and lithostratigraphy is carried out for nine sections in the Pindos foreland basin of northwest Greece, in order to generate a construction of the Pindos foreland basin during the Late Eocene and Early Oligocene.

All studied sections comprise a conspicuous change in lithology; from limestones via marl into turbiditic sandstones, and mirror the onset of siliciclastic sedimentation in the initial phase of the Pindos foreland basin development. Dinoflagellate cyst distributions suggest that:

- 1) all studied sections are of Late Eocene to Early Oligocene age (Aal to Hpu biozones)
- 2) A diachronism of 2 biozones marks the onset of siliciclastic sedimentation between the Internal and the Middle Ionian zone.

A three-dimensional reconstruction of the palaeotopography of the studied region, based on isopach data, is made. Palaeocurrent analysis suggests at least two source areas (a northern and a eastern) to be active during the initial phase of foreland basin development.

Similar and simultaneous sedimentological development of the Late Eocene to Early Oligocene sequences throughout the Pindos foreland basin suggest a relatively flat palaeotopography rather than an intensively differentiated foreland basin.

INTRODUCTION

Greece is a classic region, where origin and development of sedimentary basins, with respect to orogenesis, are intensively studied (e.g. I.F.P./I.G.R.S., 1966; Dercourt, 1977 & 1986; Aubouin, 1965). More recent works focus on the relationship between the development of foreland basins and the different stadia in the development of the Hellenic subduction zone (e.g. Meulenkamp *et al.*, 1986; Underhill, 1989). Especially the timing and magnitude of the vertical movements along and perpendicular to the Hellenic subduction zone are of great importance to identify this relationship.

In the Pindos foreland basin in northwestern Greece, a conspicuous change from limestones to siliciclastic ('flysch' type) sedimentation can be recognized. The onset of siliciclastic sedimentation is initiated by tectonic activity. Various authors (e.g. I.F.P./I.G.R.S., 1966; Bizon, 1968) dated this transition of Late Eocene to Early Oligocene age, but never focused in any detail on this transition. Little is known about sedimentation and basin configuration in the initial phase of the Pindos foreland basin development. In this study high-resolution dinoflagellate cyst stratigraphy is used to date this transition for several sections along a northeast-southwest and east-west transect. Palaeocurrent and isopach data are used to reconstruct the late Eocene to Early Oligocene basin topography.

GEOLOGICAL SETTING

The Epirus region (Figure 1), of northwest Greece is part of the Hellenide-Dinaride orogenic belt. Late Cenozoic structural evolution of western Greece involved shortening of Mesozoic passive continental-margin and Cenozoic foreland basin sequences in a foreland-propagating fold and thrust belt system. Several distinct Mesozoic facies belts have been distinguished in the (Alpine) orogenic belt of Greece on the basis of their tectonic/sedimentary history. This resulted in the recognition of isopic zones (Aubouin, 1959; 1965)(Figure 2). During the Cenozoic, deformation of these isopic zones, as a result of the scissor like closure of the Neotethyan Ocean (Dercourt, 1986), took place progressively from internal to external zones, resulting in a NNW trending mountain range.

The External Hellenides are part of the Hellenide-Dinaride orogenic belt and lie to the west of the Pindos thrust (Figure 1; Figure 2). The External Hellenides are subdivided into three isopic zones; viz the Gavrovo-Tripolitza, Ionian, and Pre-Apulian zone (Aubouin, 1959, 1965; Aubouin and Dercourt, 1962; Aubouin and others, 1976; Temple, 1968; Jenkins, 1972; Smith and Moores, 1974).

Displacement of the Pindos thrust was initiated in the middle Eocene and remained active until the Oligocene (Fleury, 1980). Foreland basin stratigraphy, consisting of a thick Oligo-

cene to early Miocene clastic wedge (the flysch of the Ionian and Gavrovo zones), was deposited on the Mesozoic to Eocene sequences (mainly carbonates) of the Outer Hellenides (Aubouin, 1959; Fleury, 1980). Clastic sedimentation of the Outer Hellenides, which started in the Late Eocene, mirrors the foreland basin development during the Oligocene and Miocene.

Palaeocurrent analysis of the Oligocene of the area of Aitolo-Akarnanian, southeast of the Gulf of Amvrakikoz (Figure 2), suggests two orientations to be significant in the infilling pattern of the Ionian basin: one axial orientation and one flow direction perpendicular to the NNW-SSE Hellenide trend (Clews, 1989; Alexander, 1990). The latter direction is suggested to reflect channelized flow off the thrust front. Axial flow pattern probably indicates strong differentiation in submarine topography along strike, as palaeocurrent data show transport in both northerly and southerly directions. Submarine topographic differentiation along strike is corroborated by the lateral variations in thickness of Oligocene and Lower Miocene deposits. Moreover lateral variations in thickness and sediment composition perpendicular to the Hellenide trend are the result of the distance to newly formed Pindos mountains (Clews, 1989).

MATERIAL

Eleven sections representing a transitional sequence from limestone to flysch sedimentation, were selected for this study (Fig.1). Nine of them were palynologically investigated. The sections were studied on their palaeocurrent markers. The sections were selected for their relatively thick sequences, which are thought to represent a complete succession. The Elati (coded: ELAT), Mazia (coded: MAZI), Arakthos (coded: ARAK), Ambelokhori (coded: AMBE) and Petrovouni (only palaeocurrent analysis) sections are situated in the Internal Ionian zone. The Agia Anastasia (coded: AYII), Dovla (coded: DOFL), Saloniki (coded: SALO), Romanos (coded: ROMA), Ekkliissia (coded: EKLN) and Polistafilon (only palaeocurrent analysis) sections are situated in the Middle Ionian zone.

The studied sections in the Internal Ionian zone belong to the "Flysch Indifférencié" formation (I.F.P./I.G.R.S., 1966), sections in the Middle Ionian zone comprise the lowermost part of the "Flysch de base" formation. The basal parts of these formations comprise the transitional sequence, which can be subdivided into four lithostratigraphic units, in ascending order:

- 1) (pelagic) limestone and/or fine grained bioclastic limestones
- 2) carbonate rich marls and lithographic limestone beds
- 3) clayey marls
- 4) alternation of sandstones and marl (flysch).

BIOSTRATIGRAPHY

Palynological sample preparation

Samples were processed using standard palynological methods that included digesting the rock in HCL and HF followed by sieving (25 μ m sieve). All samples were subjected to heavy liquid separation prior to the slide preparations. Glycerine is used as a mounting medium.

Samples and slides are stored at the Laboratory of Palaeobotany and Palynology, University of Utrecht, The Netherlands.

Counting procedures

Palynological evaluation of the samples was based on qualitative and quantitative analysis. The quantitative analysis included three steps:

- 1) Counting of the whole palynological association up to 100 palynomorphs and dividing them into four groups: viz bisaccate pollen, other pollen and spores, determinable dinoflagellate cysts (dinocysts det.), indeterminable dinoflagellates (dinocysts indet.). Undeterminable parts of dinoflagellate cysts or undeterminable cysts were attributed to the undeterminable dinoflagellate cyst group.
- 2) Counting up to 100 determinable dinoflagellate cysts. Fragments of dinoflagellate cysts which were identifiable were counted as one specimen of a certain species.
- 3) The rest of the slide was scanned to identify additional taxa.

Taxonomy corresponds to that cited in Lentini and Williams (1993).

Dinocyst zonation

The samples were dated by means of the zonal scheme set up for the Late Eocene to Early Oligocene of central- and north Italy (Fig. 3)(Brinkhuis & Biffi, 1993). A summary of their zonation is listed below:

Achomosphaera alcornu (Aal) Interval zone (uppermost Eocene-lowermost Oligocene)

Definition. The interval from the FO of *Achomosphaera alcornu* to the FO of *Glaphyrocysta semitecta*.

Remarks. *Achomosphaera* sp. (Brinkhuis and Biffi, 1993) and *Pentadinium lophophorum* appear within the zone. In addition, *Achilleodinium biformoides* reappears near the top of the zone, after a long-term absence during most part of the Late Eocene. The top of this zone is also marked by a significant increase of bisaccate pollen.

Glaphyrocysta semitecta (Gse) Interval zone (lowermost Oligocene)

Definition. The interval from the FO of *Glaphyrocysta semitecta* to the LO of *Hemiplacophora semilunifera*.

Remarks. *Achilleodinium biformoides* last occurs in this zone, whereas *Stoveracysta?* sp. appears within the zone. *Glaphyrocysta semitecta* is known to occur in the Middle to Late Eocene of the North Sea Basin (e.g. Bujak et al., 1980). However, it appears in the Mediterranean during the earliest Oligocene.

Areosphaeridium diktyoplokus (Adi) Interval zone (Lower Oligocene)

Definition. The interval from the LO of *Hemiplacophora semilunifera* to the LO of *Areosphaeridium diktyoplokus*.

Remarks. *Glaphyrocysta semitecta* becomes common to abundant within the zone. In addition, an acme of *Thalassiphora pelagica* occurs near the top of the zone.

Reticulosphaera actinocoronata (Rac) Interval zone (Lower Oligocene)

Definition. The interval from the LO of *Areosphaeridium diktyoplokus* to the LO of *Glaphyrocysta semitecta*.

Remarks. *Wetzeliiella gochtii* first occurs within this zone.

Corrudinium incompositum (Cin) Interval zone (Lower Oligocene)

Definition. The base of the zone is defined by the LO of *Glaphyrocysta semitecta*. The top is defined by the FO of *Hystrichokolpoma pusilla*.

Remarks. *Corrudinium incompositum* last occurs in the lower part of this zone, while also isolated occurrences of *Svalbardella cooksoniae* characterize that part of the zone. The upper part of the zone is characterized by the continuous occurrence of *Hystrichokolpoma* sp. of Biffi & Manum (1988), by abundant large specimens of *Reticulosphaera actinocoronata*, and by consistent occurrence of *Reticulosphaera actinocoronata* with a complete reticulum and *Wetzeliiella gochtii*. In addition *Areosphaeridium pectiniforme* gradually becomes less common in the upper part of the zone.

And finally, an new Interval zone introduced herein:

Hystrichokolpoma pusilla (Hpu) Interval zone (middle Lower Oligocene)

Definition. The base of the zone is defined by the FO of *Hystrichokolpoma pusilla*. The top of this zone is not defined.

Remarks. Continuous occurrences of *Wetzeliella gochtii* and *Hystrichokolpoma* sp. of Biffi & Manum (1988).

The precise position of the E/O boundary depends on its definition, which is still a point of discussion. In this study the E/O boundary is marked by the LO of *Areosphaeridium diktyoplokus* as proposed by Brinkhuis (1992) and therefore is placed at the top of the Adi interval zone.

RESULTS AND DISCUSSION

Nine sections were studied on their dinoflagellate cyst distribution.

Qualitative dinoflagellate cyst distribution

Ninety-four dinoflagellate cyst taxa are identified, most of them are reported by Brinkhuis & Biffi (1993). Qualitative distribution of most important marker species and of the applied dinocyst zonation are depicted in Figures 4 - 12.

The Internal Ionian zone

Reference section: Arakthos

The base of the Arakthos section is formed by the Aal zone. The top of the section is at least of Early Oligocene age (Cin interval zone). The suite of qualitative events in the Arakthos section perfectly match the zonation scheme of Brinkhuis & Biffi (1993) and Brinkhuis (1994). Some important markers found in the Arakthos section are: *Achomosphaera alvicornu*, *Tectatodinium* sp.1 *sensu* Brinkhuis and Biffi (1993), *Areosphaeridium diktyoplokus*, *Glaphyrocysta semitecta*, *Hemiplacophora semilunifera*, *Corrudinium incompositum* and *Wetzeliella gochtii*. The transition from limestones into a marly facies coincides with the Aal/Gse biozone transition (Fig. 5).

Marker species recorded in the other transitional sequences of the internal Ionian zone (Elati, Mazia and Ambelokhóri) are: *Areosphaeridium diktyoplokus* (LAD), *Wetzeliella gochtii* (FAD), *Corrudinium incompositum* (LAD) and *Glaphyrocysta semitecta* (LAD). In addition *Areosphaeridium diktyoplokus* is not reported from the Mazia section.

The data suggest that the lowermost part (limestones) of these sections is of Eocene (Aal biozone) age, while the marly and sandy upper part of these sections is of uppermost Eocene to Lower Oligocene age (Gse-Cin biozones).

The Middle Ionian zone

Reference section: Ekklissia.

Analysis of the data of the Ekklissia section suggests that the total section can be placed in an interval ranging from the Aal- or probably Gse zone to the (lower part of) Hpu zone, using presence/absence data, acme and par-acme zones. The lowermost part of the sections is assigned to the Aal-Adi biozones, while the upper part (marls and sandstones) is assigned

to the Rac-Hpu biozones (Fig. 10). Key-taxa such as *Stoveracysta* sp.1 *sensu* Brinkhuis and Biffi (1993), *Stoveracysta* sp.2 *sensu* Brinkhuis and Biffi (1993), *Heteraulacacysta leptalea*, *Areosphaeridium diktyoplokus*, *Wetziella gochti*, *Corrudinium incompositum* and *Hystrichokolpoma pusilla* provide a good basis for this zonation. On the other hand, some key-taxa observed in central Italian sections and/or sections of the Internal Ionian zone are less abundant or not observed (e.g. *Glaphyrocysta semitecta*, *Achilleodinium biformoides* and *Hemiplacophora semilunifera*).

Marker species recorded in the other transitional sequences of the middle Ionian zone (Dóvlla, Saloniki, Agia Anastasia and Romanos) are: *Areosphaeridium diktyoplokus* (LAD), *Wetziella gochti* (FAD), *Corrudinium incompositum* (LAD), *Glaphyrocysta semitecta* (LAD) and *Hystrichokolpoma pusilla* (FAD). *Areosphaeridium diktyoplokus* is not reported from the Agia Anastasia section.

Based on the qualitative dinoflagellate cysts distribution of the investigated sections it can be stated that the suite of events recorded in the Middle Ionian Zone is similar to those recorded in the Internal Ionian zone. All of the investigated sections are considered to be of Late Eocene (Priabonian) to middle Early Oligocene (middle Rupelian) age.

The transition from limestone sedimentation into clays and turbiditic sandstones, of both, the Internal and External Ionian zone during the latest Eocene and earliest Oligocene is diachronous. The first marly lithofacies occurs within different biozones. In the Internal zone this conspicuous change of sediment type coincides with the Aal/Gse biozone boundary, in the Middle Ionian zone the first marly lithofacies coincides with the Adi/Rac transition. Therefore the duration of the Gse and Adi dinocyst zones reflects the amount of diachronism.

Brinkhuis (1994) correlated the Eocene/Oligocene boundary with the Aal/Gse dinocyst zone boundary, and placed the Adi/Rac dinocyst zone boundary within chron 13n (Figure 3). According to Montanari and Odin (1988) the Eocene/Oligocene boundary is dated at 33.7 ± 0.5 Ma. Cande and Kent (1988) dated the top of chron 13 at 33.050 Ma. This implies that the maximum duration of the Gse and Adi zones is $650 \text{ Kyr} \pm 500 \text{ Kyr}$.

Quantitative dinoflagellate cyst distribution

The following genera are found to be the most abundant in the investigated sections: *Achomosphaera* - *Spiniferites* (mainly *Spiniferites ramosus* - types and *Achomosphaera alcicornu*), *Stoveracysta* (mainly *Stoveracysta* sp.1 *sensu* Brinkhuis and Biffi (1993) and *Stoveracysta* sp.2 *sensu* Brinkhuis and Biffi (1993)), *Areosphaeridium* (mainly *Areosphaeridium diktyoplokus* and *Areosphaeridium pectiniforme*), *Homotryblium* (mainly *Homotryblium aculeatum* and *Homotryblium plectilum*), *Impagidinium* (mainly *Impagidinium*

velorum and *Impagidinium* sp. *sensu* Brinkhuis and Biffi (1993), *Nematosphaeropsis* (*Nematosphaeropsis lativittatus*), *Operculodinium* (mainly *Operculodinium centrocarpum* and *Operculodinium* cf. *Operculodinium hirsutum sensu* Gocht, 1969), *Systematophora* (*Systematophora placacantha*), *Thalassiphora* (mainly *Thalassiphora pelagica*), *Deflandrea* (mainly *Deflandrea phosphoritica* and *Deflandrea arcuata*), *Tectatodinium* (mainly *Tectatodinium* sp. 2 *sensu* Brinkhuis and Biffi (1993), *Corrudinium* (mainly *Corrudinium incompositum*).

Dinoflagellate cyst distribution and terrestrial/marine ratios strongly reflect sedimentological development, bisaccate pollen and also other pollen and spores, increase significantly in an upward direction in the sections up to 70 % of palynomorphs. The lower part of the studied sections, pelagic limestones and lithographic limestones with marly intercalations, can be characterised by relative high abundances of *Impagidinium* spp. and *Nematosphaeropsis* spp: taxa mostly related to relatively open oceanic settings (e.g. Köthe, 1990; Brinkhuis, 1994; Brinkhuis and Biffi, 1993). Section upward a relative increase of marginal marine taxa is observed. *Operculodinium* spp., *Homotryblium* spp., *Deflandrea* spp. and *Spiniferites* spp. dominate these assemblages.

Lithostratigraphy

The subdivision of the transitional sequences into the four lithostratigraphic units is shown in Figures 4 - 12.

In both the Internal- and Middle Ionian zone, small sets of lithographic limestone beds (micritic, non-bioturbated limestones; lithostratigraphic unit 2)) are a characteristic feature in the transitional sequence between the (Eocene) limestone and (Oligocene) siliciclastic turbidite series . The thickness of the limestone beds vary from a few centimetres, as observed in the Ekkliissia section, to approximately 4 meters near the village of Petrouvouni and can be well correlated throughout middle and southern parts of the Internal and Middle Ionian zone. Only in the northern area (e.g. Elati section) the lithostratigraphic limestones are absent. The expected "loading effect" of the Pindos thrust on its foreland and palynological data suggest a strong relation between the formation of the lithographic limestones and considerable subsidence during the earliest Oligocene. Oost *et al.*, (in press) related the occurrence of lithographic limestones to the presence of strike-slip faults and the formation of en échelon basins with high local subsidence rates, a comparable situation to the initial phase of foreland basin development.

Palaeocurrent analysis

All sections were studied on their palaeocurrent indicators. Palaeocurrents measurements in the lowermost part of the turbiditic sandstones (within the Rac and Cin biozones) were considered to be representative for the transitional sequence. Most of the data such as grooves, furrows and lineations, to which no polarity could be ascribed, are not considered representative.

Figures 13 - 23 show the rose diagrams of the poles for the different sections. Only unidirectional data, such as flute casts and cross-bedding (foresets) were used. A listing of the data of the different sections is shown in Table 1. Circular mean, angular deviation and resultant are determined using standard statistical parameters.

Table 1. PALAEOCURRENT DATA (UNIDIRECTIONAL)

Location	n	cm.	ad.	res.	un/bi
Agia Anastasia	25	122	36.63	0.183	bi
Ambelokhori	30	269	21.16	0.727	un/bi?
Arakthos	31	322	31.04	0.413	un
Dovla	24	263	34.32	0.282	bi
Ekklessia	23	212	24.50	0.634	un
Elati	22	159	5.56	0.981	un
Mazia	12	146	9.88	0.941	un
Petrovouni	30	279	30.81	0.422	un/bi?
Polistafilon	14	224	16.03	0.844	un
Romanos	16	277	13.10	0.896	un
Saloniki	11	327	7.19	0.968	un

n = number of data

cm. = circular mean

ad. = angular deviation

res. = resultant

un/bi = unidirectional/bidirectional sediment supply.

Palaeocurrent data measured in the northern part of the Internal Ionian zone, such as the Elati and Mazia sections, indicate a sediment transport towards the southeast. In the middle part of the Internal Ionian zone the palaeocurrent data indicate sediment transport to the northwest, west and southwest.

The palaeocurrents directions in the Middle Ionian zone show a diverging pattern: in the southern part of the Middle Ionian zone, Romanos, Polistafilon and Ekklissia sections, sediment transport is predominantly trending towards the west and southwest. In the middle part of the Middle Ionian zone, Saloniki and Dovla, the predominant palaeocurrent direction is towards the northwest. In addition, in the Dovla and Agia Anastasia sections, a bidirectional system of sediment supply is recorded suggesting sediment sources in the east (Pindos mountains) and in north of Epirus.

No change in trend in palaeocurrent is observed within one section. The dominant palaeocurrent direction within a section is depicted in Figure 25.

Palaeocurrent distribution and isopach data

In an attempt to reconstruct the foreland basin geometry, the dominant palaeocurrent data were compared with isopach data of the Eocene limestone (data of I.F.P./I.G.R.S., 1966). We considered the isopach data (Figure 24) to reflect the basin morphology during the Eocene. Because of the pelagic nature of the Eocene limestones, the thickest package represents the deepest parts of the basin. In this study a linear relation between basin topography, at the end of the Eocene, and underlying thickness of the Eocene sequence is assumed.

Analysis of palaeocurrent data suggest that the Epirus region can be divided into two depositional areas: the northern part dominated by axial flow, the southern part dominated by a transverse flow of sediment. The data also indicate that sediment supply originated in different source areas, one located in the north and one in the eastern part of the Pindos mountains. The apex of the distributary system of the eastern source area was probably situated between the village of Pramada (Ambelokhori) and Petrovouni as palaeocurrent data indicate a diverging pattern (Figure 25). It is not clear whether the northern source area is located towards the northeast (Pindos zone) or more to the northwest (Albania), possibly indicating an elevated area as the result of halokinesis or tectonic uplift. In the southern depositional area, palaeocurrents are deflected in either northern or southern direction in the middle Ionian zone which may indicate a relatively elevated area in the west.

CONCLUSIONS

The transitional sequence from limestone sedimentation into siliciclastic sedimentation in the Pindos foreland basin comprises the Aal to Hpu dinoflagellate cyst zones (Late Eocene to Early Oligocene). The lower part of the transitional sequence is characterised by relative high abundances of outer neritic and oceanic taxa whereas the upper part of the sequence is dominated by relatively marginal marine taxa.

The onset of siliciclastic sedimentation in the Pindos foreland basin is diachronous. In the Internal Ionian zone this conspicuous change coincides with the Aal/Gse biozone boundary, in the Middle Ionian Zone with the Adi/Rac biozone boundary. Calibration of these zones, using palaeomagnetic data, provides a diachronism of 650 +/- 500 Kyr.

Palaeocurrent data imply that the Pindos foreland basin can be subdivided into two depositional domains: the northern domain characterized by axial flow from the north and the southern domain characterized by sediment flow from the east. No distinct lithological difference is observed between both systems.

A three dimensional reconstruction of the Pindos foreland basin, suggests relatively elevated areas in the northwest and northeast. In the northern part of the Pindos foreland, sediment flow reflects the presence of intra-basinal ridges parallel to the thrust front. In contrast, the southern area, where palaeorelief is less distinct, a more dispersed pattern of palaeocurrents is observed

The transitional sequences in both Internal and Middle Ionian zone are comparable with respect to their sedimentological development, suggesting a relatively smoothly curved and well connected foreland. Deposition of lithographic limestones can be interpreted in terms of high local subsidence rates in the initial phase of foreland basin development, and coincides with and increase of oceanic taxa in the dinoflagellate cyst assemblage.

ACKNOWLEDGEMENTS

Special thanks go to the Molengraaff foundation, for financial support of this work. Henk Brinkhuis, Henk Visscher, Johan Meulenkamp, Hans Zyderveld, Roel Verreussel and Han Leereveld are kindly thanked for their constructive discussions and helpful suggestions and comments. The co-workers of the Laboratory of Palaeobotany and Palynology of the University of Utrecht and co-workers of the LPP-Foundation are kindly thanked for their interest in this work. The authors acknowledge support from the LPP-Foundation.

SPECIES LIST

List of encountered dinoflagellate cysts.

Achomosphaera alvicornu
Areoligera sentosa
Areosphaeridium diktyoplokus
Areosphaeridium pectiniforme
Caligodinium amiculum
Charlesdowniea clathrata
Cordosphaeridium cantharellum
Corrudinium sp. 2 Head & Norris, 1989
Corrudinium incompositum
Dapsilidinium pseudocolligerum
Deflandrea arcuata
Deflandrea granulata
Deflandrea heterophlycta
Deflandrea phosphoritica
Deflandrea sp. cf. *D. heterophlycta*
Deflandrea spinulosa
Dinopterigium cladoides sensu Morgenroth, 1966
Diphyes colligerum
Distatodinium craterum
Distatodinium ellipticum
Distatodinium tenerum
Fibrocyta axialis
Glaphyrocysta semitecta
Hemiplacophora semilunifera
Heteraulacacysta campanula
Heteraulacacysta leptalea
Homotryblium abbreviatum
Homotryblium aculeatum
Homotryblium floripes
Homotryblium pallidum
Homotryblium plectilum.
Hystrichokolpoma rigaudiae
Hystrichokolpoma salacia
Hystrichokolpoma sp. Biffi & Manum, 1988
Hystrichosphaeropsis rectangularis
Impagidinium brevisulcatum
Impagidinium dispertitum
Impagidinium pallidum
Impagidinium sp. Brinkhuis & Biffi, 1993
Impagidinium sp. cf. *I. aculeatum* (Wall) Lentin & Williams, 1981
Impagidinium velorum
Lentinia serrata
Lingulodinium pycnospinosum
Nematosphaeropsis lemniscata
Operculodinium centrocarpum
Operculodinium cf. *O. hirsutum sensu* Gocht, 1969
Operculodinium microtriainum
Operculodinium tiara
Palaeocystodinium golzowense
Pentadinium circumsutum
Pentadinium goniferum
Pentadinium laticinctum

Rottnestia borussica
Samlandia chlamydophora
Schematophora speciosa
Spiniferites cornutus
Spiniferites membranaceus
Spiniferites mirabilis
Spiniferites perforatus
Spiniferites pseudofurcatus
Spiniferites ramosus granosus
Spiniferites ramosus ramosus
Spiniferites rectangularis
Spiniferites sp. 1
Spiniferites verrucatus
Stoveracysta sp. 1 Brinkhuis & Biffi, 1993
Stoveracysta sp. 2 Brinkhuis & Biffi, 1993
Stoveracysta sp. 3
Systematophora ancyrea
Systematophora placacantha
Tectatodinium pellitum
Tectatodinium sp. 1 Brinkhuis & Biffi, 1993
Tectatodinium sp. 2 Brinkhuis & Biffi, 1993
Thalassiphora delicata
Thalassiphora pelagica
Thalassiphora succincta
Turbiosphaera symmetrica
Wetzeliella articulata
Wetzeliella gochtii

REFERENCES

- Alexander, J., Nichols, G.J. and Leigh, S., 1990. The origin of marine conglomerates in the Pindus foreland basin, Greece. *Sedimentary geology*, 66, p. 243-254.
- Aubouin, J., 1959. Contribution à l'étude géologique de la Grèce septentrionale: les confirm de l'Épire et de la Thessalie. *Ann. Geol. des Pays Hellen.*, 10, 483 pp., Athens.
- Aubouin, J. and Dercourt, J., 1962. Zone préapulienne, zone ionienne et zone du Gavrovo en Peloponnese occidentale. *Bulletin de Société Géologique de France*, v. 4.
- Aubouin, J., 1965. Contribution à l'étude géologique de la Grèce septentrionale: les confirm de l'Épire et de la Thessalie. *Geosynclines: Amsterdam, New York, Elsevier Publishing Company*, 335 p..
- Aubouin, J. et al., 1976. Esquisse structurale de l'arc Egéen externe: des Dinarides aux Taurides. *Bulletin de Société Géologique de France*, v. 7, no. 43.
- Biffi, U. and Manum, S.B., 1988. Late Eocene-Early Miocene dinoflagellate cyst biostratigraphy from the Marche Region (Central Italy). *Bull. Soc. Pal. Ital. (Modena)*, 27, 2, pp. 163-212.
- Bizon, J. 1967. Contribution a la connaissance des Foraminifères planctonique d'Épire et des îles ioniennes (Grèce occidentale) depuis le Paléogène jusqu'au Pliocène. *Paris Technip, Ph.D. thesis*.
- Brinkhuis, H., 1992. Late Eocene to Early Oligocene dinoflagellate cysts from central and northeast Italy. *Thesis*.
- Brinkhuis, H. and Biffi, U., 1993. Dinoflagellate cyst stratigraphy of the Eocene/Oligocene transition in central Italy. *Marine Micropaleontology*.
- Brinkhuis, H., 1994. Late Eocene to Early Oligocene dinoflagellate cysts from the Priabonian type-area (Northeast Italy): biostratigraphy and palaeoenvironmental interpretation. *Palaeogeography, Palaeoclimatology, Palaeoecology*.
- Bujak, J.P., Downie, C., Eaton, G.L. and Williams, G.L., 1980. Dinoflagellate cysts and acritarchs from the Eocene of southern England. *The Palaeontological Association, special papers in Paleontology* 24, 100 p..
- Cande, S.C. and Kent, D.V., 1992. A new geomagnetic polarity time scale for the Late Cretaceous and Cenozoic. *Journal of geophysical research*. 97, p. 13971-13951.
- Clews, J.E., 1989. Structural controls on basin evolution: Neogene to Quaternary of the Ionian zone, Western Greece. *Journal of the Geological Society, London*, p. 447-457.

Dercourt, J., Aubouin, J., Savoyat, E. *et al.*, 1977. Réunion extraordinaire de la société géologique en Grèce. *Bull.Soc.géol. France.*, 19, p. 5-70

Dercourt, J., Zonenshain, L.P. *et al.*, 1986. Geological evolution of the Tethys belt from the Atlantic to the Pamirs since the Lias. *Tectonophysics* 123: 241-315.

Fleury, J.J., 1980. Les zones de Gavrovo-Tripolitza et du Pinde-Olonus (Grèce occidentale et Peloponèse du Nord). Evolution d'une plate-forme et d'un bassin dans leur cadre alpin. *Special Publication de Société Géologique du Nord*, no. 4.

I.F.P./I.G.R.S., 1966. Etude géologique de l'Épire. *Inst. Français Pétrole*, Editions Technip, 306 pp, Paris.

Jenkins, D.A.L., 1972. Structural development of western Greece. *Am. Ass. Petrol. Geol. Bull.*, v. 56, 128-149.

Köthe, A., 1990. Paleogene dinoflagellates from northwest Germany. *Geol. Jahrb.*, 118, 111p.

Meulenkamp, J.E., Wortel, M.J.R., Van Wamel, W.A., Spakman, W., Hoogerduyn Strating, E., 1986, On the Hellenic subduction zone and the geodynamic evolution of Crete since the late Middle Miocene. *Tectonophysics*, 146, 146, p. 203-215.

Lentin, J.K. and Williams, G.L., 1993. Fossil dinoflagellates: index to genera and species. *AASP contribution series*, 28: 856 pp.

Montanari, A. *et al.*, 1988. Radioisotopic dating of the Eocene-Oligocene boundary in the pelagic sequence of the northeastern Apennines. In: I.Premoli Silva, R. Coccioni and A. Montanari (Editors), The Eocene-Oligocene boundary in the Marche-Umbria Basin (Italy). *International Union of Geological Sciences Commission on Stratigraphy; International Subcommittee on Paleogene Stratigraphy Report* (Ancona, Italy, 1988), pp.195-205.

Oost, A.P. and De Boer, P.L., (in press). Tectonic and climatic setting of lithographic limestone basins. *Geobios*. no.16.

Smith, A.G. and Moores, E.M., 1974. Hellenides. In *Spencer A.M. ed.. Mesozoic and Cenozoic orogenic belts. Geological Society of London Special Publication*, 4, p. 159-185.

Temple, P.G., 1968. Mechanics of large-scale gravity sliding in the Greek Peloponnesos. *Geol. Soc. Am. Bull.*, v. 79, p. 687-700.

Underhill, J.R., 1989. Late Cenozoic deformation of the Hellenide foreland, western Greece. *Geol. Soc. Am. Bull.*, v.101, p.613-634.

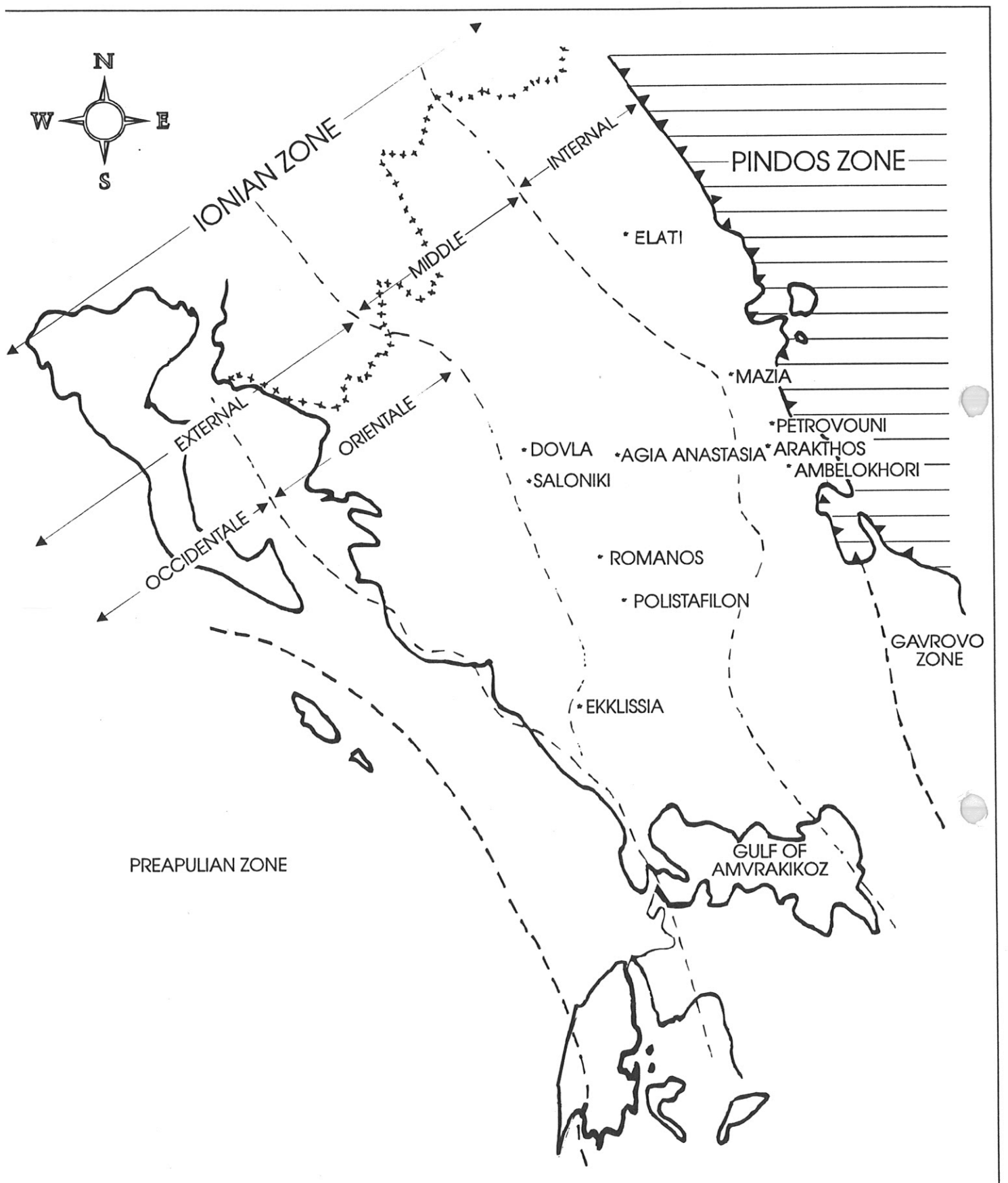


Figure 1. Epirus region and location of sections.

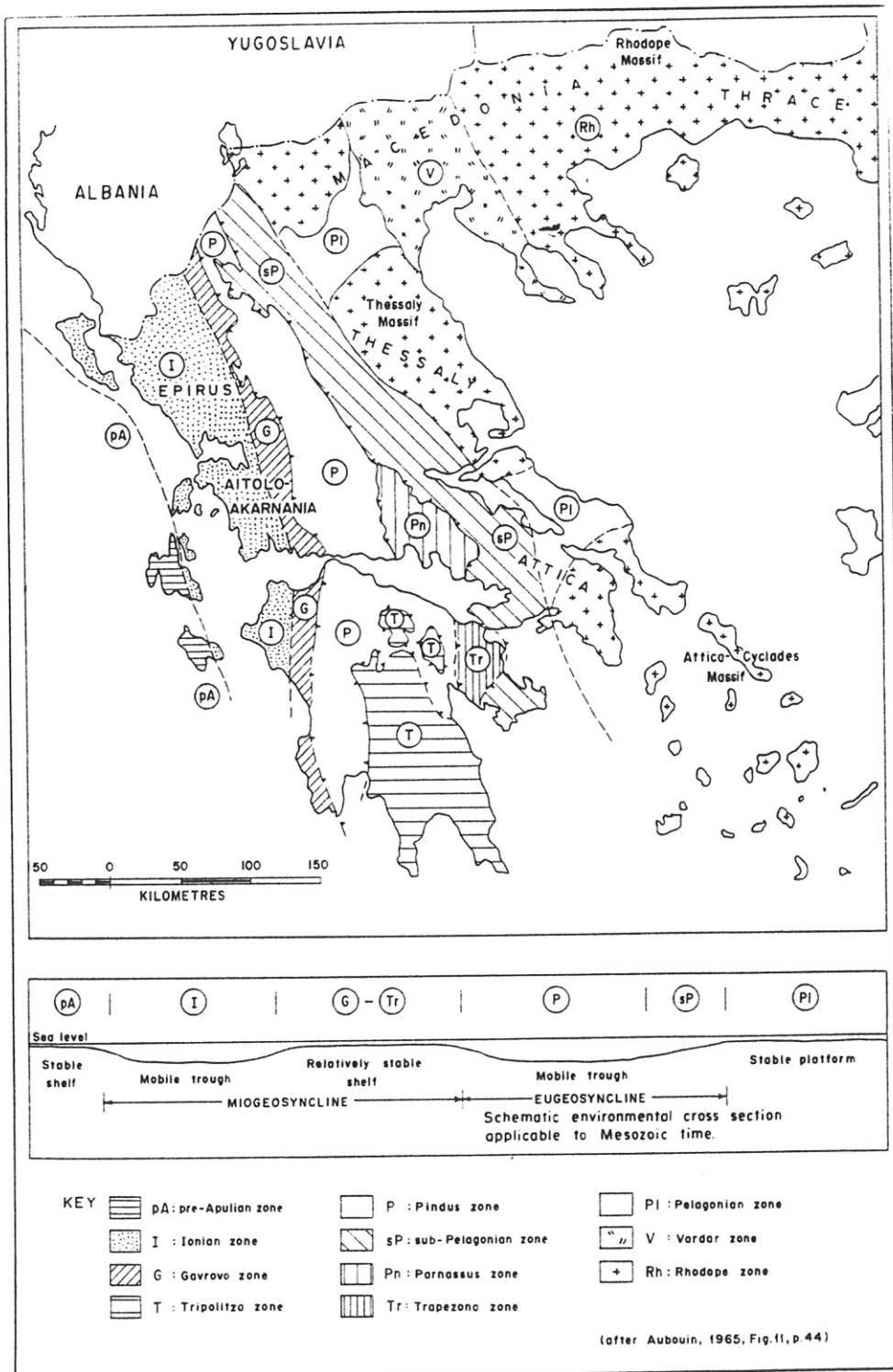


Figure 2. Isopic zones of sedimentation. After Aubouin, 1965.

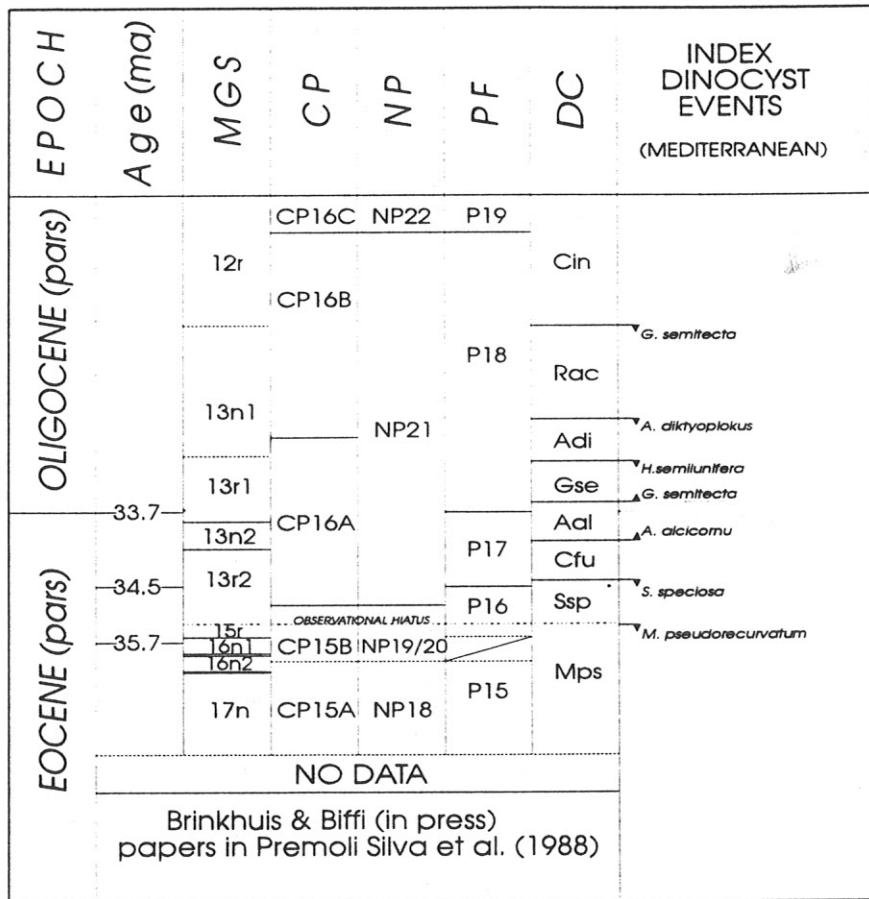

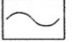

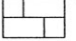
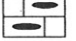

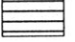




Figure 3. Dinoflagellate cyst (DC) zonation of investigated sections in central Italy with schematic composite diagram of the correlatable bio- and magnetostratigraphies, from Brinkhuis and Biffi (1993). *PF* = standard planktonic foraminifer zones (after Blow, 1969, and Nocchi *et al.*, 1988a,b); *NP* = standard nannoplankton zones (after Martini, 1971); *CP* = standard nannoplankton zones (after Okada and Bukry, 1980); *MGS* = magnetostratigraphy obtained from the Massignano section; all *PF*, *NP*, *CP* and *MGS*-data from papers in Premoli-Silva *et al.* (1988a); *DC* = dinoflagellate cyst zonation (Brinkhuis and Biffi, 1993).

LITHOLOGY		SYMBOLS	
	SANDSTONE	FU	FINING UPWARD BED
	MARL		CHANNEL
	LIMESTONE	M	MARKER BED
	LIMESTONE WITH CHERT LENSES	F	FAULT
FACIES			
UNIT 4		CLAY AND TURBIDITIC SANDSTONE FACIES	
UNIT 3		MARL / CLAY FACIES	
UNIT 2		LIMESTONE / MARL ALTERNATION FACIES	
UNIT 1		LIMESTONE FACIES	

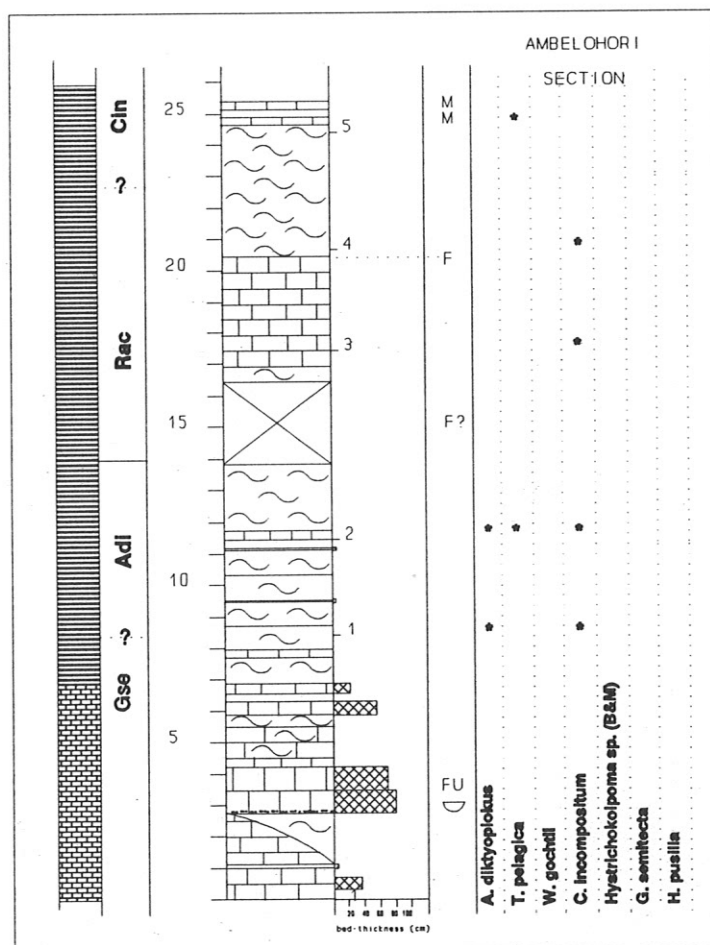


Figure 4. Lithostratigraphy and dinocyst zonation of the Ambelokhori section.

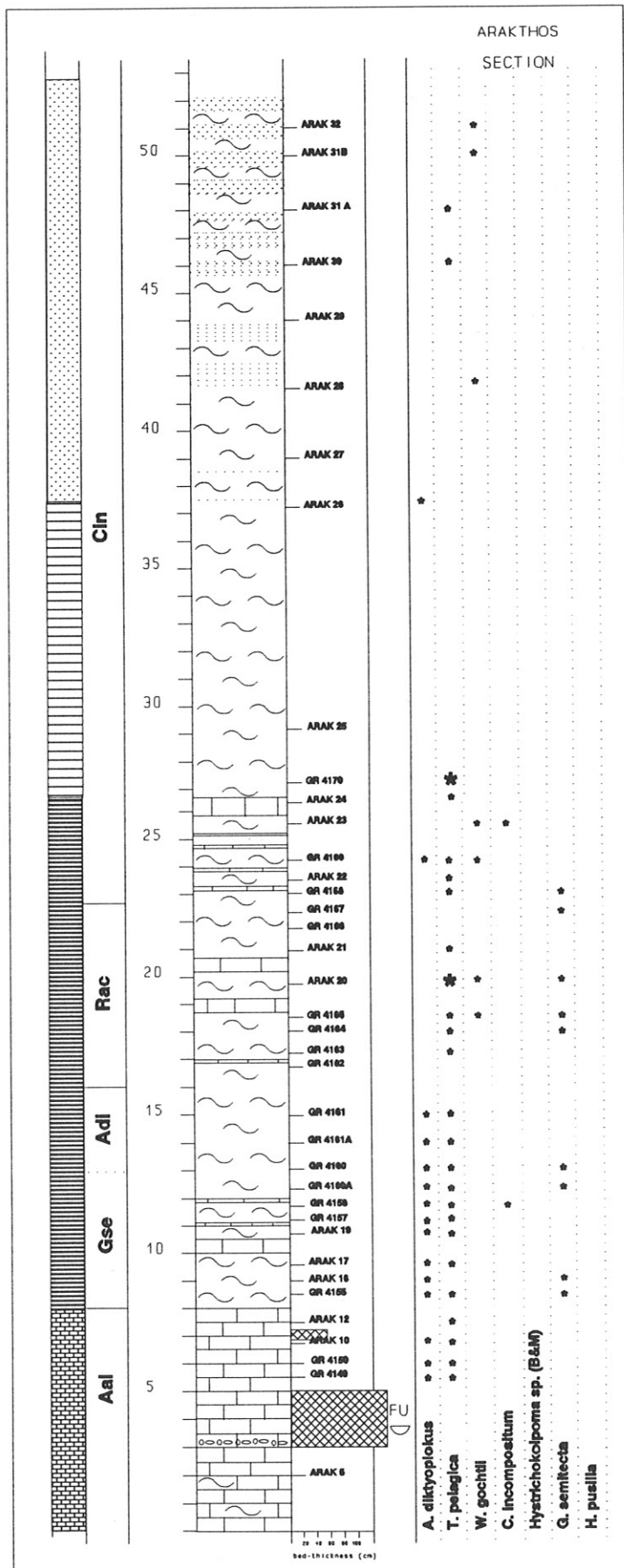


Figure 5. Lithostratigraphy and dinocyst zonation of the Arakthos section.

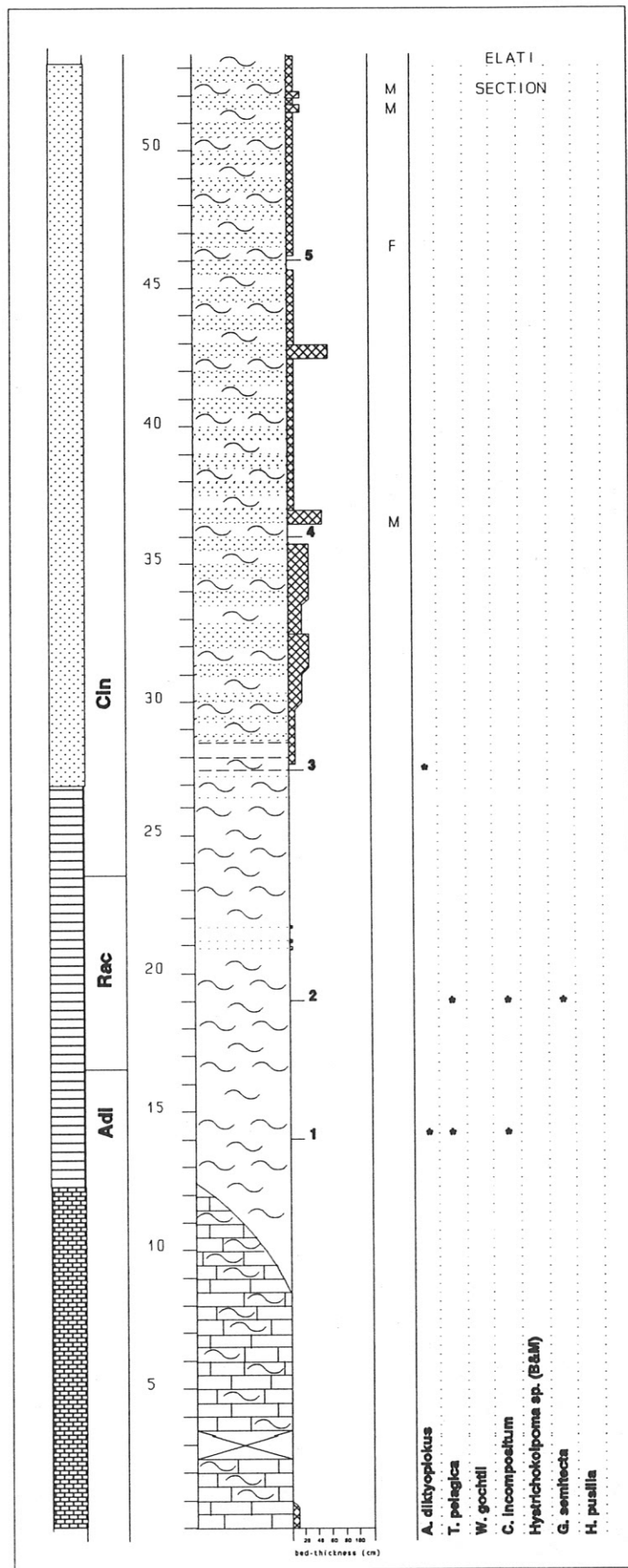


Figure 6. Lithostratigraphy and dinocyst zonation of the Elati section.

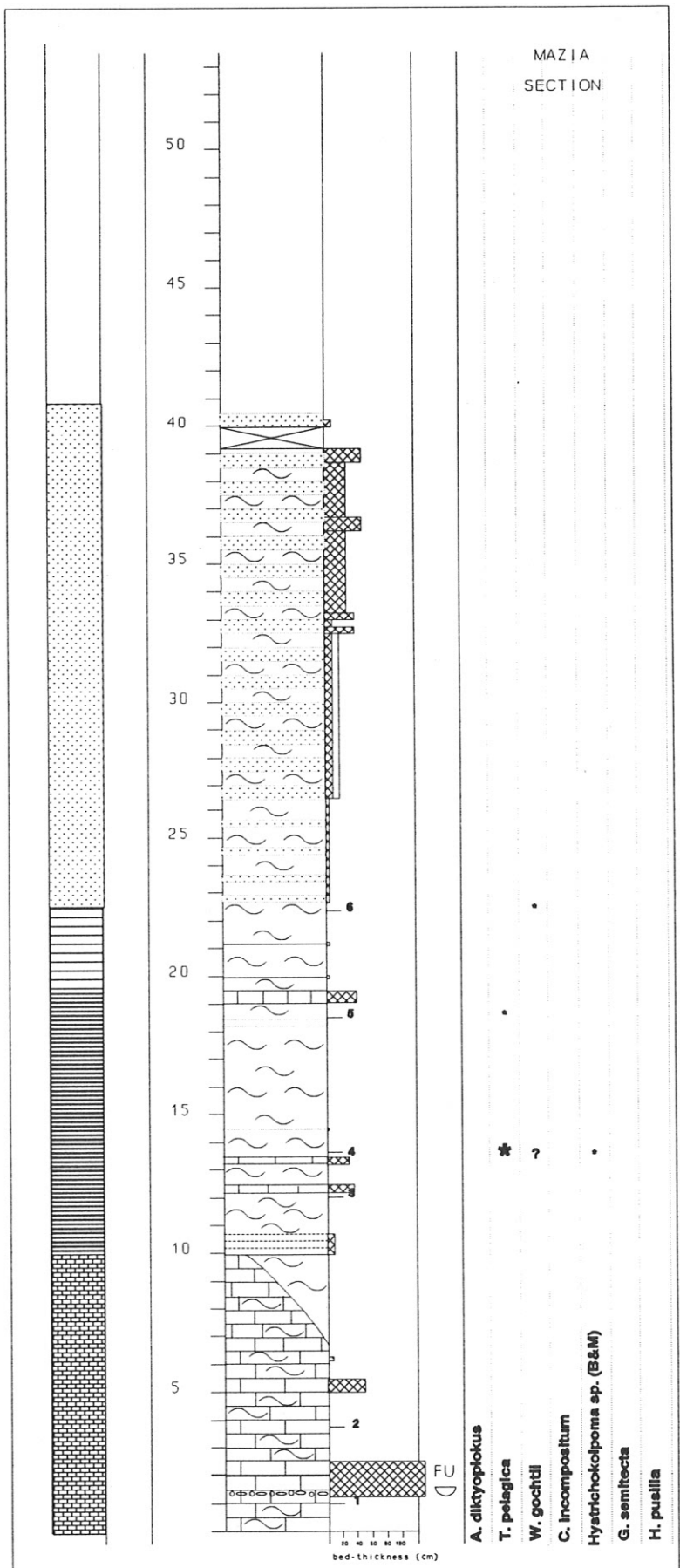


Figure 7. Lithostratigraphy of the Mazia section.

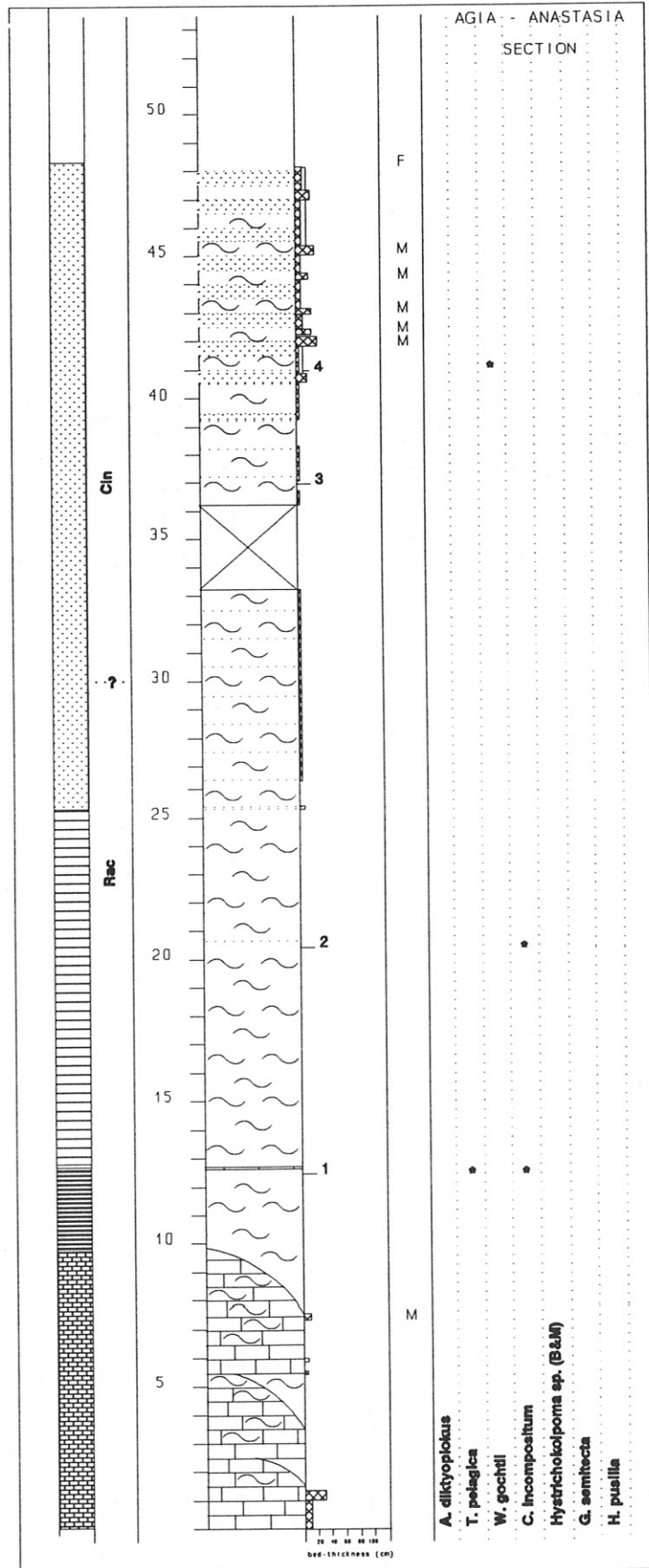


Figure 8. Lithostratigraphy and dinocyst zonation of the Agia - Anastasia section.

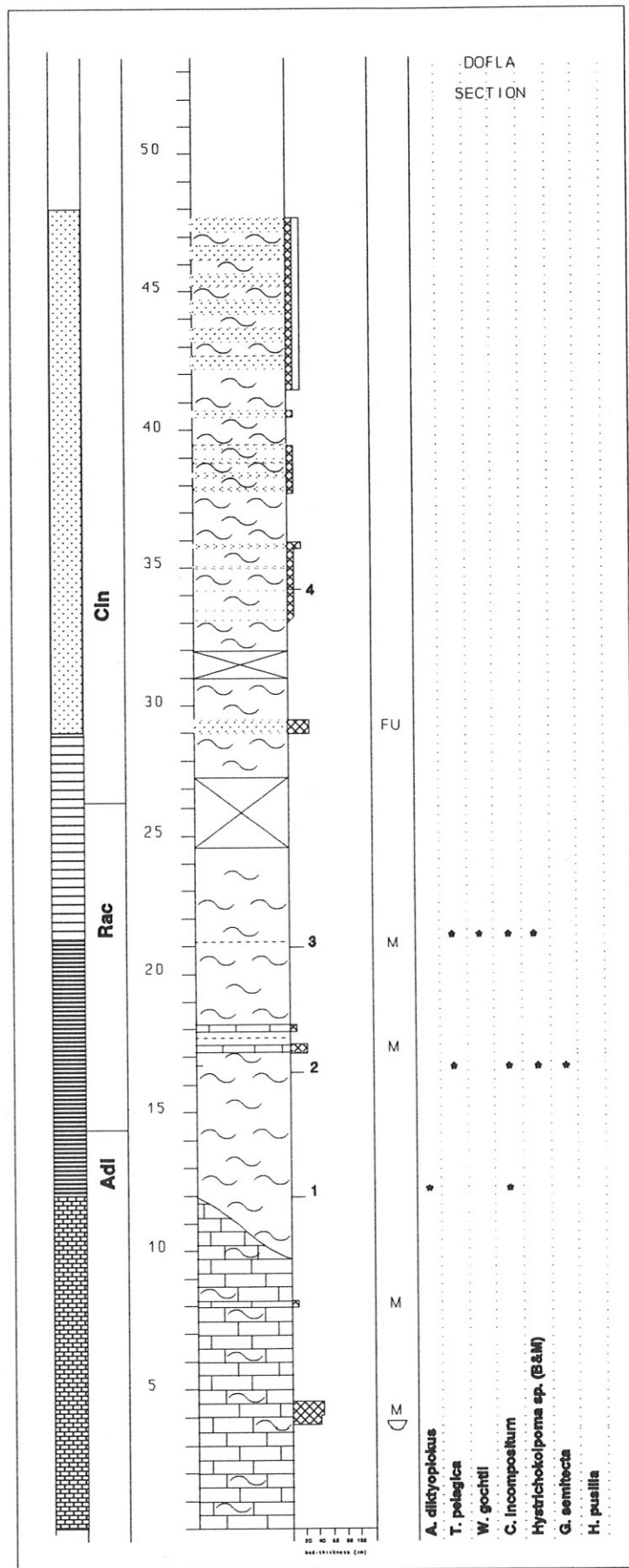


Figure 9. Lithostratigraphy and dinocyst zonation of the Dofla section.

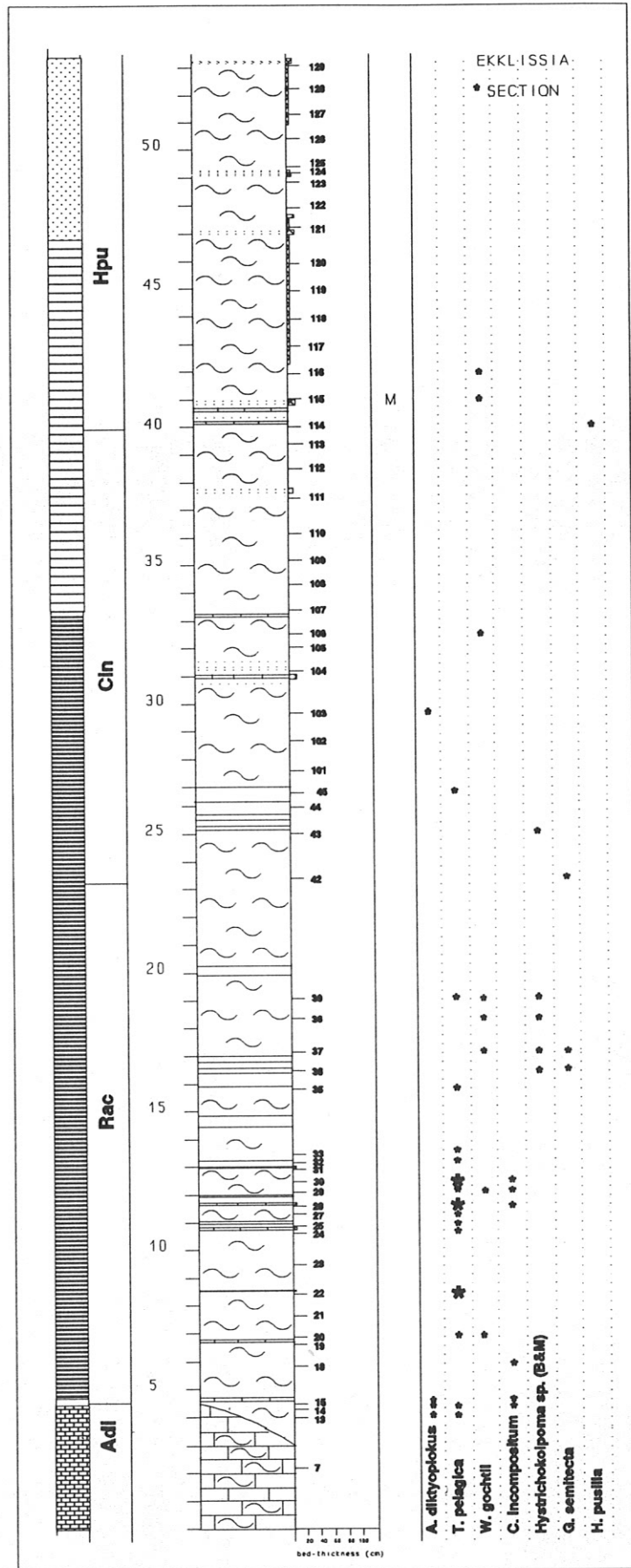


Figure 10. Lithostratigraphy and dinocyst zonation of the Ekklesia section.

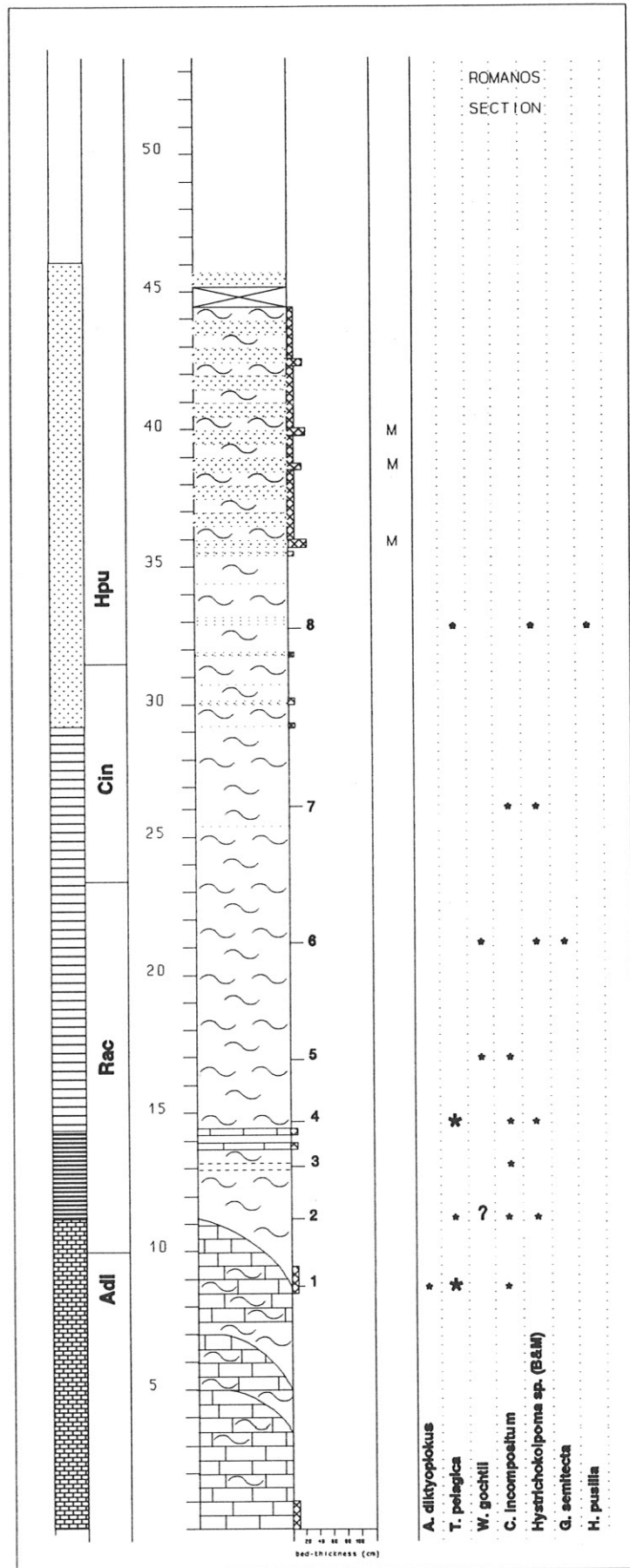


Figure 11. Lithostratigraphy and dinocyst zonation of the Romanos section.

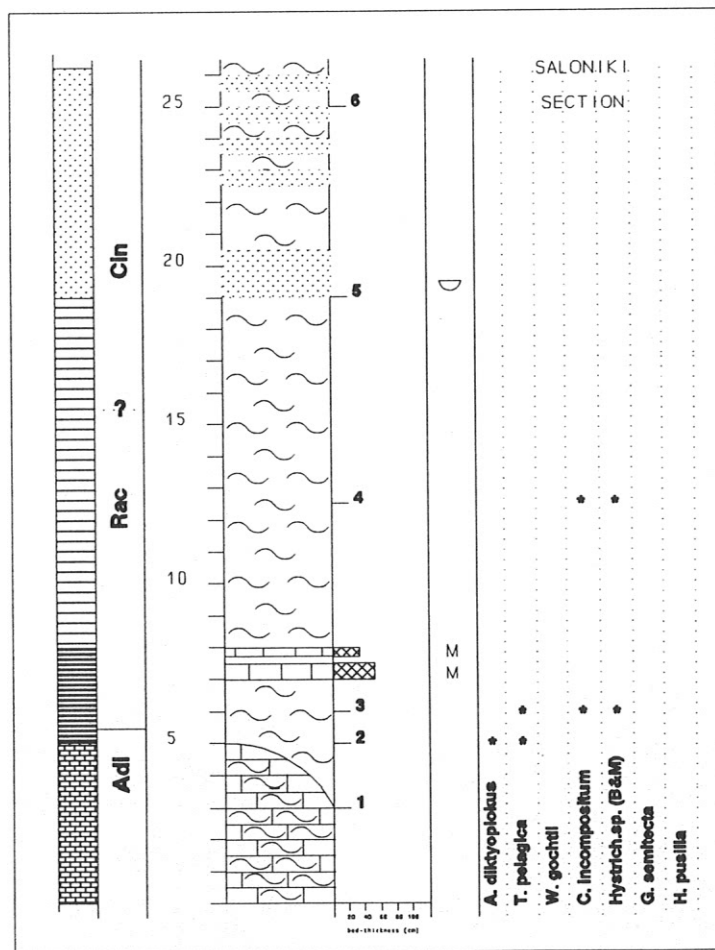
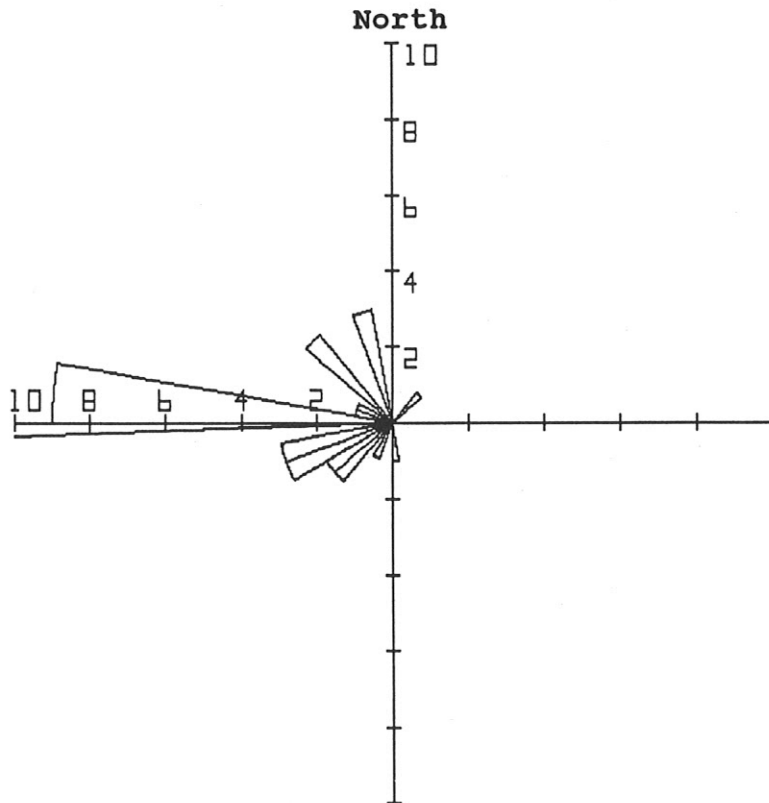


Figure 12. Lithostratigraphy and dinocyst zonation of the Saloniki section.

ROSE DIAGRAM OF POLE TREND FOR
palaeocurrents Ambelokhori section



30 Data Points
Single Line Shows Vector Mean

Circular Mean = 269 degree(s)
Angular Dev. = 21.16
Resultant = 0.727

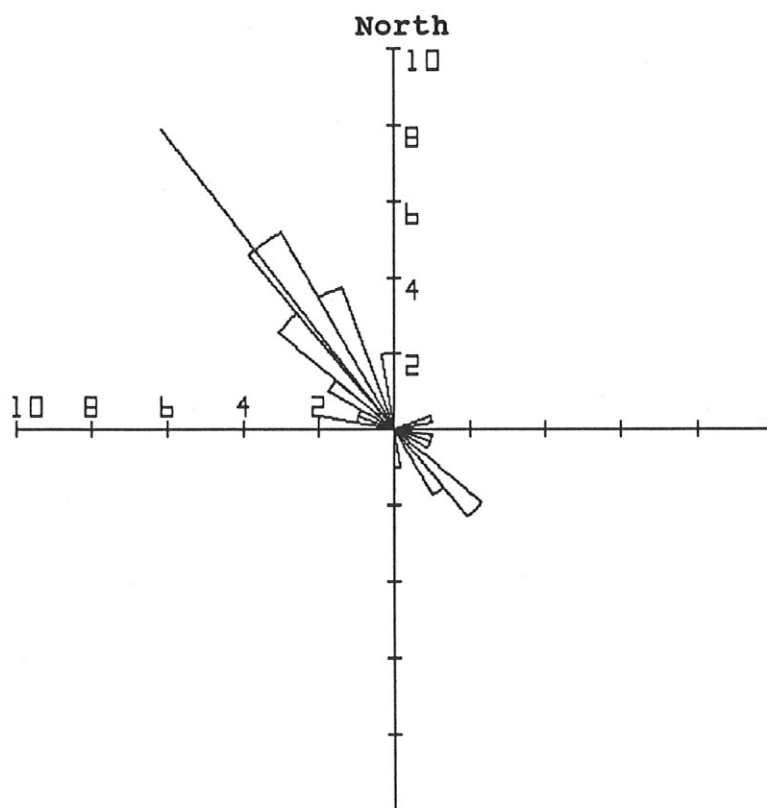
BREAKDOWN OF 10x SECTORS:

Range (deg)	Number	% of Total	3	Range (deg)	Number	% of Total
0- 9	0	0	3	180-189	0	0
10- 19	0	0	3	190-199	0	0
20- 29	0	0	3	200-209	1	3
30- 39	0	0	3	210-219	0	0
40- 49	1	3	3	220-229	2	7
50- 59	0	0	3	230-239	2	7
60- 69	0	0	3	240-249	3	10
70- 79	0	0	3	250-259	3	10
80- 89	0	0	3	260-269	0	0
90- 99	0	0	3	270-279	9	30
100-109	0	0	3	280-289	1	3
110-119	0	0	3	290-299	1	3
120-129	0	0	3	300-309	0	0
130-139	0	0	3	310-319	3	10
140-149	0	0	3	320-329	0	0
150-159	0	0	3	330-339	0	0
160-169	0	0	3	340-349	3	10
170-179	1	3	3	350-360	0	0

SPLIT by Darton Software

Figure 13.

ROSE DIAGRAM OF POLE TREND FOR
palaeocurrents Arakthos section



31 Data Points
Single Line Shows Vector Mean

Circular Mean = 322 degree(s)
Angular Dev. = 31.04
Resultant = 0.413

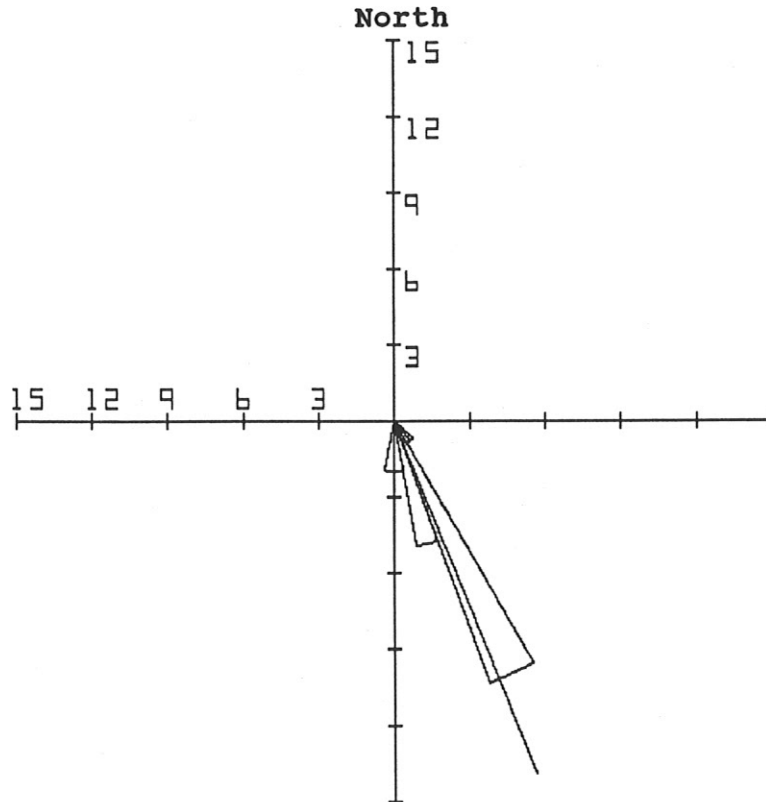
BREAKDOWN OF 10x SECTORS:

Range (deg)	Number	% of Total	3	Range (deg)	Number	% of Total
0- 9	0	0	3	180-189	0	0
10- 19	0	0	3	190-199	0	0
20- 29	0	0	3	200-209	0	0
30- 39	0	0	3	210-219	0	0
40- 49	0	0	3	220-229	0	0
50- 59	0	0	3	230-239	0	0
60- 69	0	0	3	240-249	0	0
70- 79	1	3	3	250-259	0	0
80- 89	0	0	3	260-269	0	0
90- 99	0	0	3	270-279	2	6
100-109	1	3	3	280-289	1	3
110-119	1	3	3	290-299	1	3
120-129	0	0	3	300-309	2	6
130-139	3	10	3	310-319	4	13
140-149	2	6	3	320-329	6	19
150-159	0	0	3	330-339	4	13
160-169	0	0	3	340-349	0	0
170-179	1	3	3	350-360	2	6

SPLIT by Darton Software

Figure 14.

ROSE DIAGRAM OF POLE TREND FOR
palaeocurrents Elati section



22 Data Points
Single Line Shows Vector Mean

Circular Mean = 159 degree(s)
Angular Dev. = 5.56
Resultant = 0.981

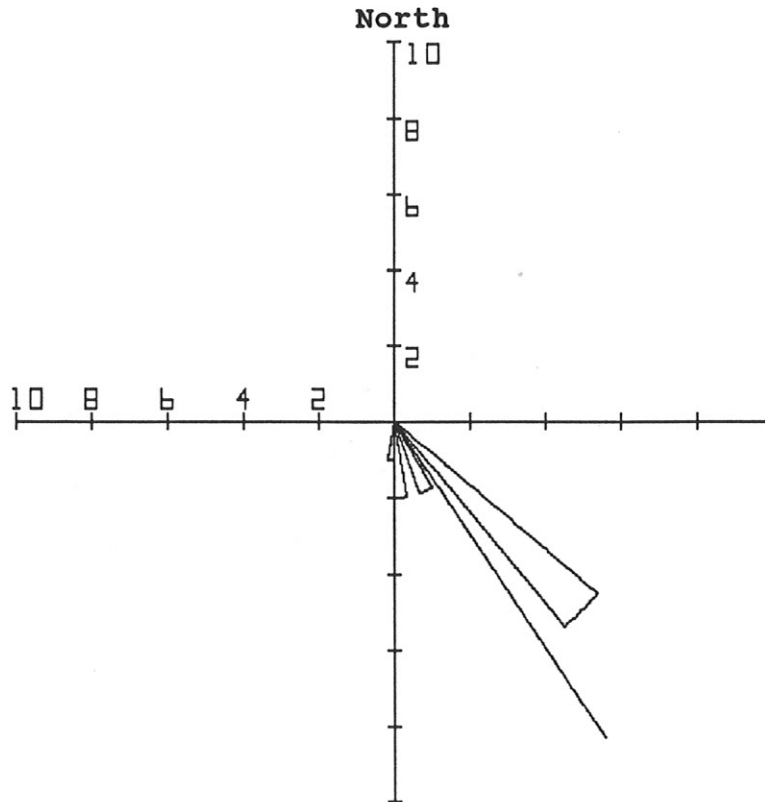
BREAKDOWN OF 10x SECTORS:

Range (deg)	Number	% of Total	3	Range (deg)	Number	% of Total
0- 9	0	0	3	180-189	2	9
10- 19	0	0	3	190-199	0	0
20- 29	0	0	3	200-209	0	0
30- 39	0	0	3	210-219	0	0
40- 49	0	0	3	220-229	0	0
50- 59	0	0	3	230-239	0	0
60- 69	0	0	3	240-249	0	0
70- 79	0	0	3	250-259	0	0
80- 89	0	0	3	260-269	0	0
90- 99	0	0	3	270-279	0	0
100-109	0	0	3	280-289	0	0
110-119	0	0	3	290-299	0	0
120-129	0	0	3	300-309	0	0
130-139	1	5	3	310-319	0	0
140-149	1	5	3	320-329	0	0
150-159	11	50	3	330-339	0	0
160-169	5	23	3	340-349	0	0
170-179	2	9	3	350-360	0	0

SPLIT by Darton Software

Figure 15.

ROSE DIAGRAM OF POLE TREND FOR
palaeocurrents Mazia section



12 Data Points
Single Line Shows Vector Mean

Circular Mean = 146 degree(s)
Angular Dev. = 9.88
Resultant = 0.941

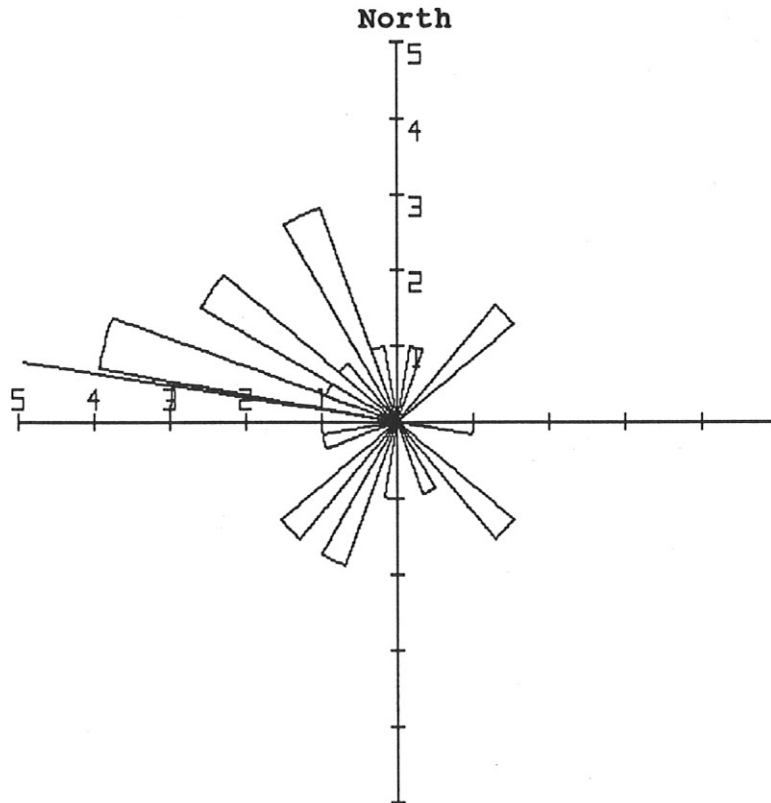
BREAKDOWN OF 10x SECTORS:

Range (deg)	Number	% of Total	3	Range (deg)	Number	% of Total
0- 9	0	0	3	180-189	1	8
10- 19	0	0	3	190-199	0	0
20- 29	0	0	3	200-209	0	0
30- 39	0	0	3	210-219	0	0
40- 49	0	0	3	220-229	0	0
50- 59	0	0	3	230-239	0	0
60- 69	0	0	3	240-249	0	0
70- 79	0	0	3	250-259	0	0
80- 89	0	0	3	260-269	0	0
90- 99	0	0	3	270-279	0	0
100-109	0	0	3	280-289	0	0
110-119	0	0	3	290-299	0	0
120-129	0	0	3	300-309	0	0
130-139	7	58	3	310-319	0	0
140-149	0	0	3	320-329	0	0
150-159	2	17	3	330-339	0	0
160-169	0	0	3	340-349	0	0
170-179	2	17	3	350-360	0	0

SPLIT by Darton Software

Figure 16.

ROSE DIAGRAM OF POLE TREND FOR
palaeocurrents Petrovouni section



30 Data Points
Single Line Shows Vector Mean

Circular Mean = 279 degree(s)
Angular Dev. = 30.81
Resultant = 0.422

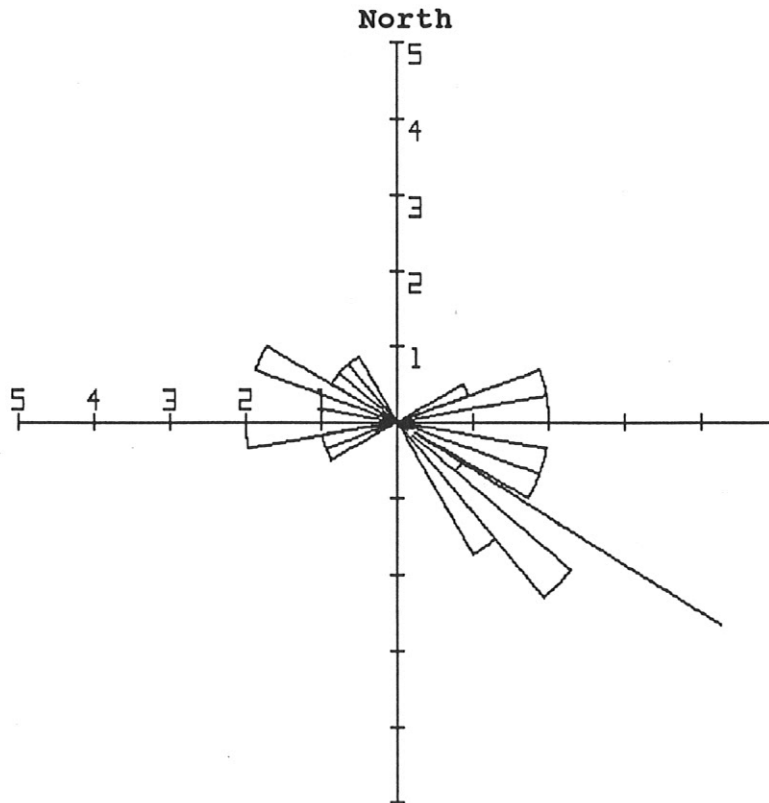
BREAKDOWN OF 10x SECTORS:

Range (deg)	Number	% of Total	3	Range (deg)	Number	% of Total
-----	-----	-----	3	-----	-----	-----
0- 9	0	0	3	180-189	1	3
10- 19	1	3	3	190-199	0	0
20- 29	0	0	3	200-209	2	7
30- 39	0	0	3	210-219	0	0
40- 49	2	7	3	220-229	2	7
50- 59	0	0	3	230-239	0	0
60- 69	0	0	3	240-249	0	0
70- 79	0	0	3	250-259	1	3
80- 89	0	0	3	260-269	1	3
90- 99	1	3	3	270-279	3	10
100-109	0	0	3	280-289	4	13
110-119	0	0	3	290-299	1	3
120-129	0	0	3	300-309	3	10
130-139	2	7	3	310-319	1	3
140-149	0	0	3	320-329	0	0
150-159	1	3	3	330-339	3	10
160-169	0	0	3	340-349	1	3
170-179	0	0	3	350-360	0	0

SPLIT by Darton Software

Figure 17.

ROSE DIAGRAM OF POLE TREND FOR
palaeocurrents Agia Anastasia section



25 Data Points
Single Line Shows Vector Mean

Circular Mean = 122 degree(s)
Angular Dev. = 36.63
Resultant = 0.183

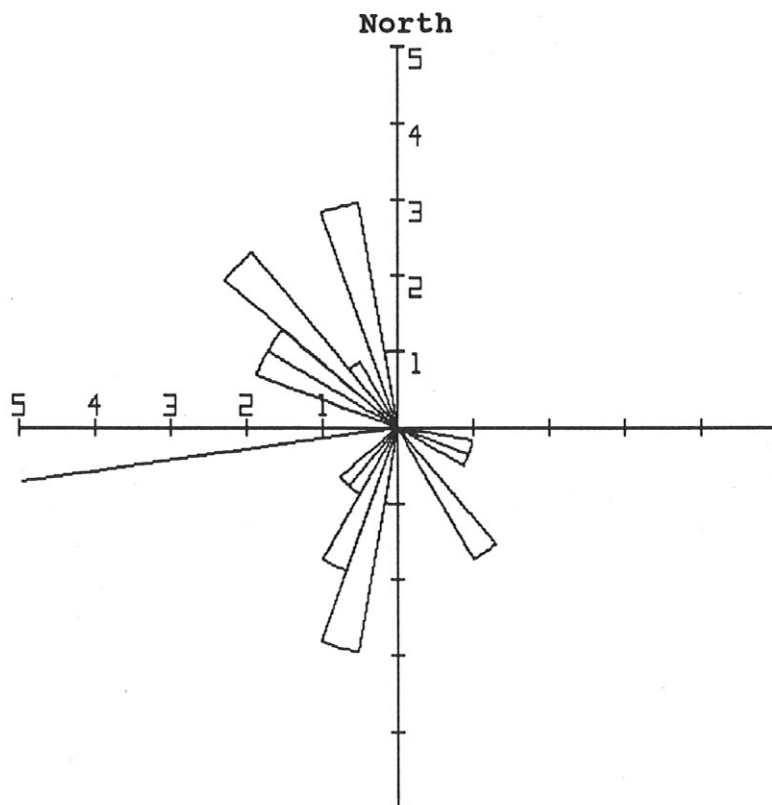
BREAKDOWN OF 10x SECTORS:

Range (deg)	Number	% of Total	3	Range (deg)	Number	% of Total
0- 9	0	0	3	180-189	0	0
10- 19	0	0	3	190-199	0	0
20- 29	0	0	3	200-209	0	0
30- 39	0	0	3	210-219	0	0
40- 49	0	0	3	220-229	0	0
50- 59	0	0	3	230-239	0	0
60- 69	1	4	3	240-249	1	4
70- 79	2	8	3	250-259	1	4
80- 89	2	8	3	260-269	2	8
90- 99	0	0	3	270-279	1	4
100-109	2	8	3	280-289	0	0
110-119	2	8	3	290-299	2	8
120-129	1	4	3	300-309	1	4
130-139	3	12	3	310-319	1	4
140-149	2	8	3	320-329	1	4
150-159	0	0	3	330-339	0	0
160-169	0	0	3	340-349	0	0
170-179	0	0	3	350-360	0	0

SPLOT by Darton Software

Figure 18.

ROSE DIAGRAM OF POLE TREND FOR
Palaeocurrents Dofla section



24 Data Points
Single Line Shows Vector Mean

Circular Mean = 263 degree(s)
Angular Dev. = 34.32
Resultant = 0.282

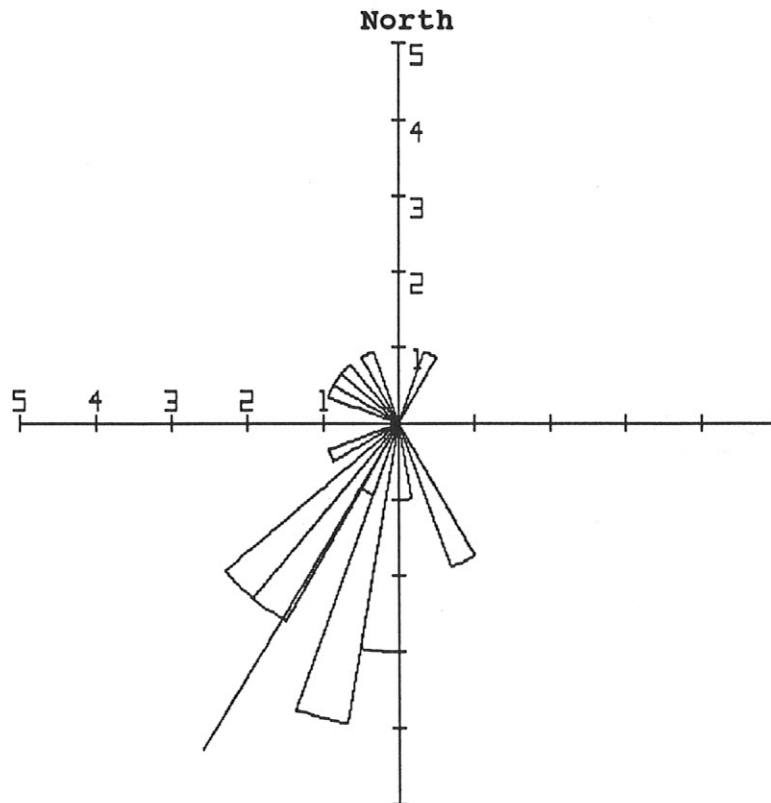
BREAKDOWN OF 10x SECTORS:

Range (deg)	Number	% of Total	3	Range (deg)	Number	% of Total
0- 9	0	0	3	180-189	1	4
10- 19	0	0	3	190-199	3	13
20- 29	0	0	3	200-209	2	8
30- 39	0	0	3	210-219	1	4
40- 49	0	0	3	220-229	1	4
50- 59	0	0	3	230-239	0	0
60- 69	0	0	3	240-249	0	0
70- 79	0	0	3	250-259	0	0
80- 89	0	0	3	260-269	0	0
90- 99	0	0	3	270-279	0	0
100-109	1	4	3	280-289	0	0
110-119	1	4	3	290-299	2	8
120-129	0	0	3	300-309	2	8
130-139	0	0	3	310-319	3	13
140-149	2	8	3	320-329	1	4
150-159	0	0	3	330-339	0	0
160-169	0	0	3	340-349	3	13
170-179	0	0	3	350-360	1	4

SPLIT by Darton Software

Figure 19.

ROSE DIAGRAM OF POLE TREND FOR
palaeocurrents Eklissia section



23 Data Points
Single Line Shows Vector Mean

Circular Mean = 212 degree(s)
Angular Dev. = 24.50
Resultant = 0.634

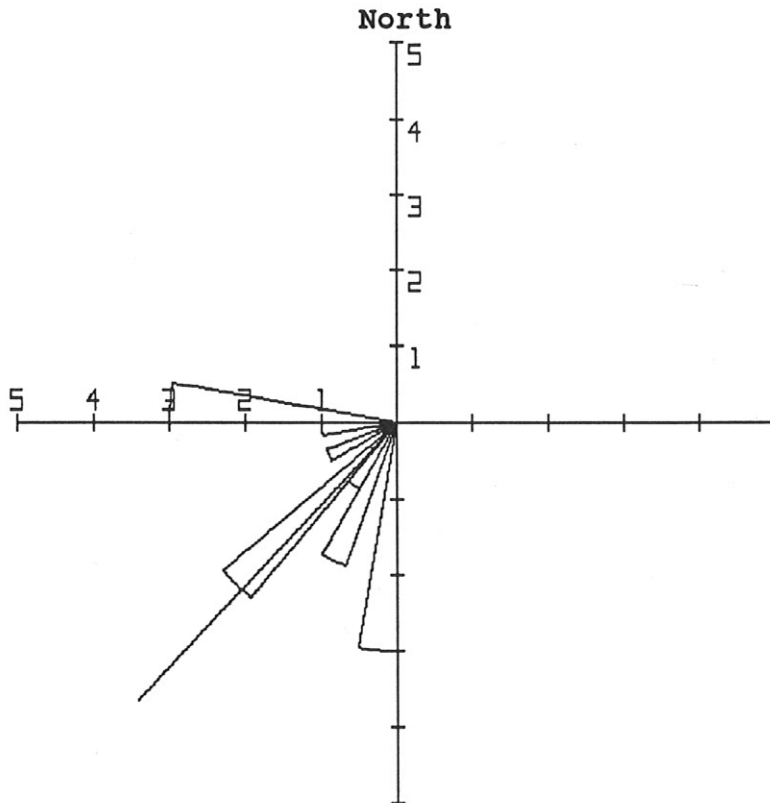
BREAKDOWN OF 10x SECTORS:

Range (deg)	Number	% of Total	3	Range (deg)	Number	% of Total
0- 9	0	0	3	180-189	3	13
10- 19	0	0	3	190-199	4	17
20- 29	1	4	3	200-209	1	4
30- 39	0	0	3	210-219	3	13
40- 49	0	0	3	220-229	3	13
50- 59	0	0	3	230-239	0	0
60- 69	0	0	3	240-249	1	4
70- 79	0	0	3	250-259	0	0
80- 89	0	0	3	260-269	0	0
90- 99	0	0	3	270-279	0	0
100-109	0	0	3	280-289	0	0
110-119	0	0	3	290-299	1	4
120-129	0	0	3	300-309	1	4
130-139	0	0	3	310-319	1	4
140-149	0	0	3	320-329	0	0
150-159	2	9	3	330-339	1	4
160-169	0	0	3	340-349	0	0
170-179	1	4	3	350-360	0	0

SPLIT by Darton Software

Figure 20.

ROSE DIAGRAM OF POLE TREND FOR
palaeocurrents Polistafilon section



14 Data Points
Single Line Shows Vector Mean

Circular Mean = 224 degree(s)
Angular Dev. = 16.03
Resultant = 0.844

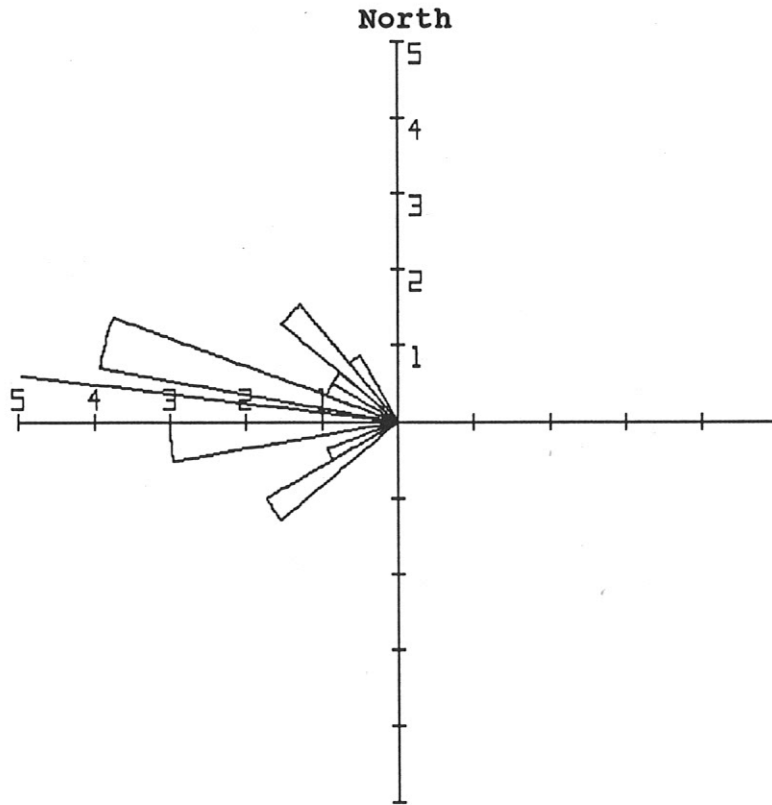
BREAKDOWN OF 10x SECTORS:

Range (deg)	Number	% of Total	3	Range (deg)	Number	% of Total
0- 9	0	0	3	180-189	3	21
10- 19	0	0	3	190-199	0	0
20- 29	0	0	3	200-209	2	14
30- 39	0	0	3	210-219	1	7
40- 49	0	0	3	220-229	3	21
50- 59	0	0	3	230-239	0	0
60- 69	0	0	3	240-249	1	7
70- 79	0	0	3	250-259	0	0
80- 89	0	0	3	260-269	1	7
90- 99	0	0	3	270-279	3	21
100-109	0	0	3	280-289	0	0
110-119	0	0	3	290-299	0	0
120-129	0	0	3	300-309	0	0
130-139	0	0	3	310-319	0	0
140-149	0	0	3	320-329	0	0
150-159	0	0	3	330-339	0	0
160-169	0	0	3	340-349	0	0
170-179	0	0	3	350-360	0	0

SPLIT by Darton Software

Figure 21.

ROSE DIAGRAM OF POLE TREND FOR
palaeocurrents Romanos section



16 Data Points
Single Line Shows Vector Mean

Circular Mean = 277 degree(s)
Angular Dev. = 13.10
Resultant = 0.896

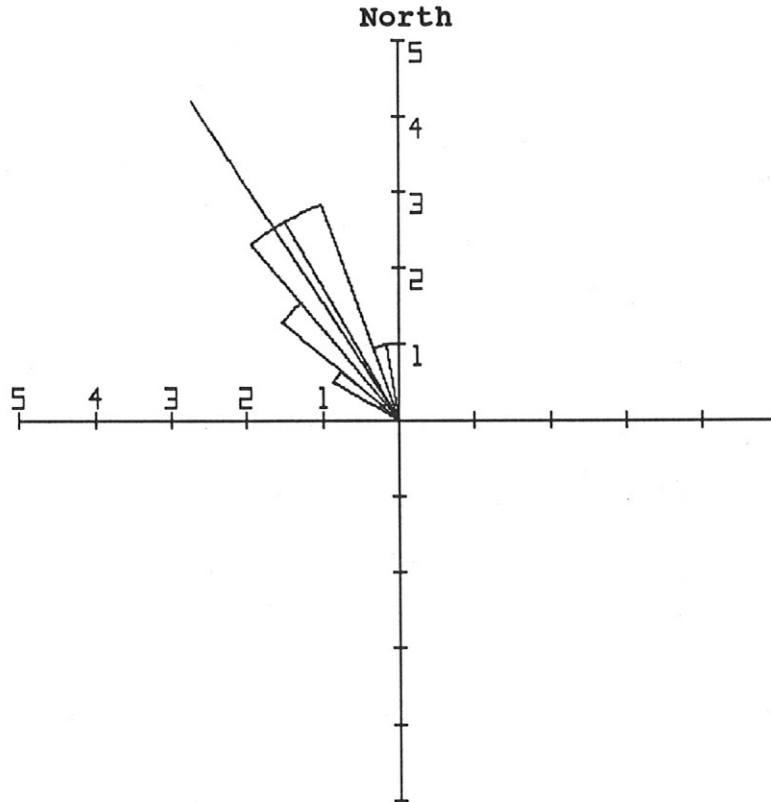
BREAKDOWN OF 10x SECTORS:

Range (deg)	Number	% of Total	3	Range (deg)	Number	% of Total
-----	-----	-----	3	-----	-----	-----
0- 9	0	0	3	180-189	0	0
10- 19	0	0	3	190-199	0	0
20- 29	0	0	3	200-209	0	0
30- 39	0	0	3	210-219	0	0
40- 49	0	0	3	220-229	0	0
50- 59	0	0	3	230-239	2	13
60- 69	0	0	3	240-249	1	6
70- 79	0	0	3	250-259	0	0
80- 89	0	0	3	260-269	3	19
90- 99	0	0	3	270-279	1	6
100-109	0	0	3	280-289	4	25
110-119	0	0	3	290-299	1	6
120-129	0	0	3	300-309	1	6
130-139	0	0	3	310-319	2	13
140-149	0	0	3	320-329	1	6
150-159	0	0	3	330-339	0	0
160-169	0	0	3	340-349	0	0
170-179	0	0	3	350-360	0	0

SPLIT by Darton Software

Figure 22.

ROSE DIAGRAM OF POLE TREND FOR
palaeocurrents Saloniki section



11 Data Points
Single Line Shows Vector Mean

Circular Mean = 327 degree(s)
Angular Dev. = 7.19
Resultant = 0.968

BREAKDOWN OF 10x SECTORS:

Range (deg)	Number	% of Total	3	Range (deg)	Number	% of Total
0- 9	0	0	3	180-189	0	0
10- 19	0	0	3	190-199	0	0
20- 29	0	0	3	200-209	0	0
30- 39	0	0	3	210-219	0	0
40- 49	0	0	3	220-229	0	0
50- 59	0	0	3	230-239	0	0
60- 69	0	0	3	240-249	0	0
70- 79	0	0	3	250-259	0	0
80- 89	0	0	3	260-269	0	0
90- 99	0	0	3	270-279	0	0
100-109	0	0	3	280-289	0	0
110-119	0	0	3	290-299	0	0
120-129	0	0	3	300-309	1	9
130-139	0	0	3	310-319	2	18
140-149	0	0	3	320-329	3	27
150-159	0	0	3	330-339	3	27
160-169	0	0	3	340-349	1	9
170-179	0	0	3	350-360	1	9

SPLIT by Darton Software

Figure 23.

ISOPACH MAP OF EOCENE LIMESTONE

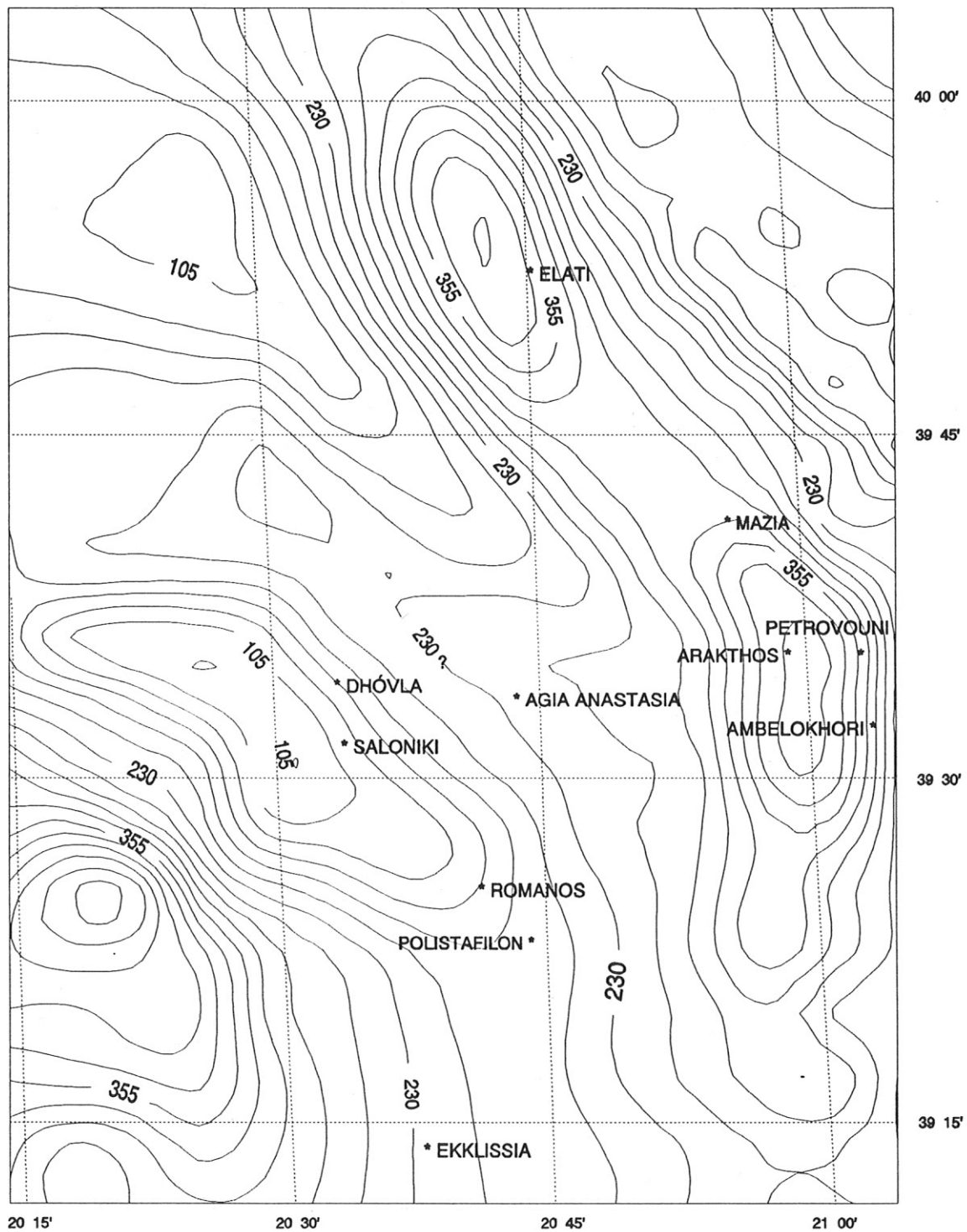


Figure 24. Isopach map of Eocene limestone.

3-D RECONSTRUCTION OF THE
 PINDOS FORELAND BASIN
 AT THE EOCENE OLIGOCENE BOUNDARY

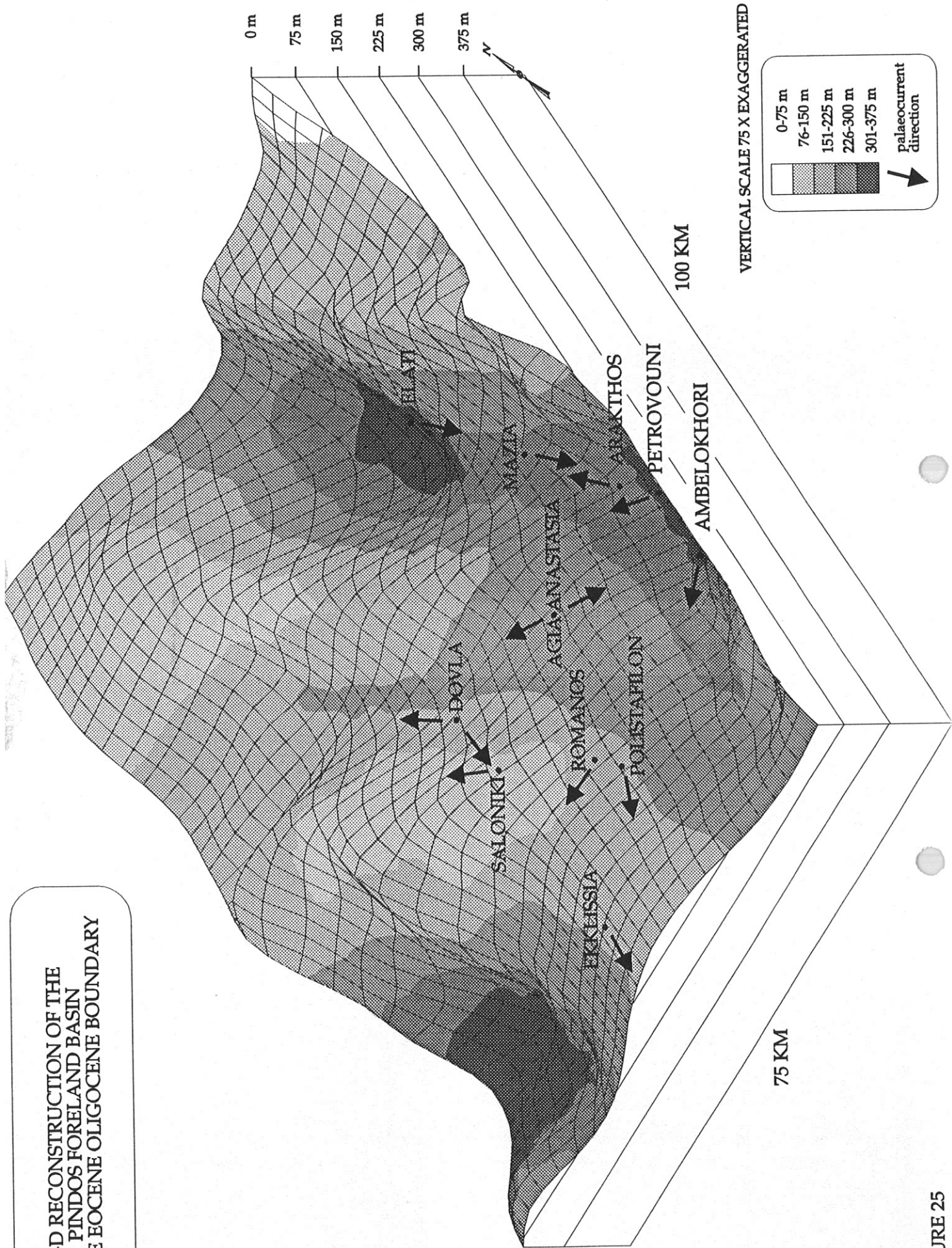


FIGURE 25

